INFORMATION TO USERS

This dissertation was produced from a microfilm copy of the original document. While the most advanced technological means to photograph and reproduce this document have been used, the quality is heavily dependent upon the quality of the original submitted.

The following explanation of techniques is provided to help you understand markings or patterns which may appear on this reproduction.

1. The sign or "target" for pages apparently lacking from the document photographed is "Missing Page(s)". If it was possible to obtain the missing page(s) or section, they are spliced into the film along with adjacent pages. This may have necessitated cutting thru an image and duplicating adjacent pages to insure you complete continuity.

2. When an image on the film is obliterated with a large round black mark, it is an indication that the photographer suspected that the copy may have moved during exposure and thus cause a blurred image. You will find a good image of the page in the adjacent frame.

3. When a map, drawing or chart, etc., was part of the material being photographed the photographer followed a definite method in "sectioning" the material. It is customary to begin photoing at the upper left hand corner of a large sheet and to continue photoing from left to right in equal sections with a small overlap. If necessary, sectioning is continued again — beginning below the first row and continuing on until complete.

4. The majority of users indicate that the textual content is of greatest value, however, a somewhat higher quality reproduction could be made from "photographs" if essential to the understanding of the dissertation. Silver prints of "photographs" may be ordered at additional charge by writing the Order Department, giving the catalog number, title, author and specific pages you wish reproduced.

University Microfilms

300 North Zeeb Road
Ann Arbor, Michigan 48106

A Xerox Education Company

THE UNIVERSITY OF OKLAHOMA

GRADUATE COLLEGE

AUGER ELECTRON SPECTROSCOPY OF THE LANTHANIDE RARE EARTH ELEMENTS

A DISSERTATION

SUBMITTED TO THE GRADUATE FACULTY

in partial fulfillment of the requirements for the

degree of

DOCTOR OF PHILOSOPHY

BY

KENNETH PAUL MADDOX

Norman, Oklahoma

AUGER ELECTRON SPECTROSCOPY OF THE LANTHANIDE RARE EARTH ELEMENTS

APPROVED BY

DISSERTATION COMMITTEE

ACKNOWLEDGEMENTS

The author expresses his appreciation to Dr. R. C. Jerner for help and encouragement during this project. Dr. A. W. Aldag spent many hours in discussion and review of the results. Dr. R. J. Block was graciously cooperative in preparing photographic reproductions.

The National Science Foundation provided the financial support of a traineeship during the bulk of these studies.

Last, both thanks and apology are due to family and friends, who bore with tact the periods of preoccupation and irritability attending this work's completion.

TABLE OF CONTENTS

LIST OF TABLES

LIST OF FIGURES

ABSTRACT

Auger Electron Spectroscopy (AES) has been used to investigate the Lanthanide rare earth series. Spectra obtained with a cylindrical mirror analyzer have been identified in X-ray notation for transitions between atomic energy levels. Systematic shifts in energy with increasing atomic number have been tabulated and described. Intensity variations between peaks are shown in reproduced spectra and described in semiquantitative terms.

Ionization loss peaks have been used to identify transitions and supplement X-ray data for the lower energy levels. Comparison between the data reveals large differences for energies less than 160 eV. Calculated Auger energies are shown to be in close agreement with experiment only if ionization loss data is employed.

Calibration of Auger energies by reference to elastic backscattered electrons is discussed. A constant difference of 4-5 eV is found between Auger energies thus calibrated and previously reported data.

CHAPTER I

AUGER ELECTRON SPECTROSCOPY

INTRODUCTION

Auger Electron Spectroscopy (AES) uses the characteristic kinetic energy of Auger secondary electrons to identify surface species. An electron-stimulated secondary emission spectrum (Fig. 1) includes a true secondary background, an elastic peak, characteristic ionization losses due to interaction of the primary beam with target atoms, plasmon losses and gains--the result of quantum transfers to and from quantized electron cloud vibrations, and Auger electrons. The last are produced during the return of ionized atoms to ground state. The process (Fig. 2) involves in general an initial ionization W, electron transition from energy level X, and emission of an electron bound in level Y. A WXY Auger electron has kinetic energy

$$KE_A = E_W - E_X - E_Y$$

where E_W, E_X, and E_Y are energies for levels W, X, and Y, respectively.

To the first approximation W, X, and Y are X-ray atomic energy levels, and the WXY notation employs X-ray designations K, L_1, L_2, L_3, M_1, etc. The error in using atomic levels for ions is apparent. To calculate Auger energies E_Y is generally modified[1] to

$$E'_Y(Z) = E_Y(Z) + \Delta Z[E_Y(Z + 1) - E_Y(Z)]$$

where ΔZ is an empirically determined variable between 0 and 1.0--usually 0.7, $E_Y(Z + 1)$ and $E_Y(Z)$ are the energies of the Y atomic energy level for elements Z and Z + 1, respectively. A further correction[2] symmetrizes the Auger energy

$$KE_A = E_W - E'_X - E'_Y$$

since the atomic energy states after both WXY and WYX transitions are equal, doubly ionized in the X and Y levels. Good agreement has been shown[2,3] between empirical and calculated data. The use of notation, calculations and X-ray atomic energy level data is discussed for the rare earth series in Chapters II, IV, and V.

Auger electrons are usually produced by low energy electron or X-ray excitation. The secondary electron spectrum is energy analyzed by retardation or deflection of emitted secondaries. The latter method is used in the cylindrical mirror analyzer (Fig. 4), which features high speed energy discrimination while retaining good resolution.[5-9]

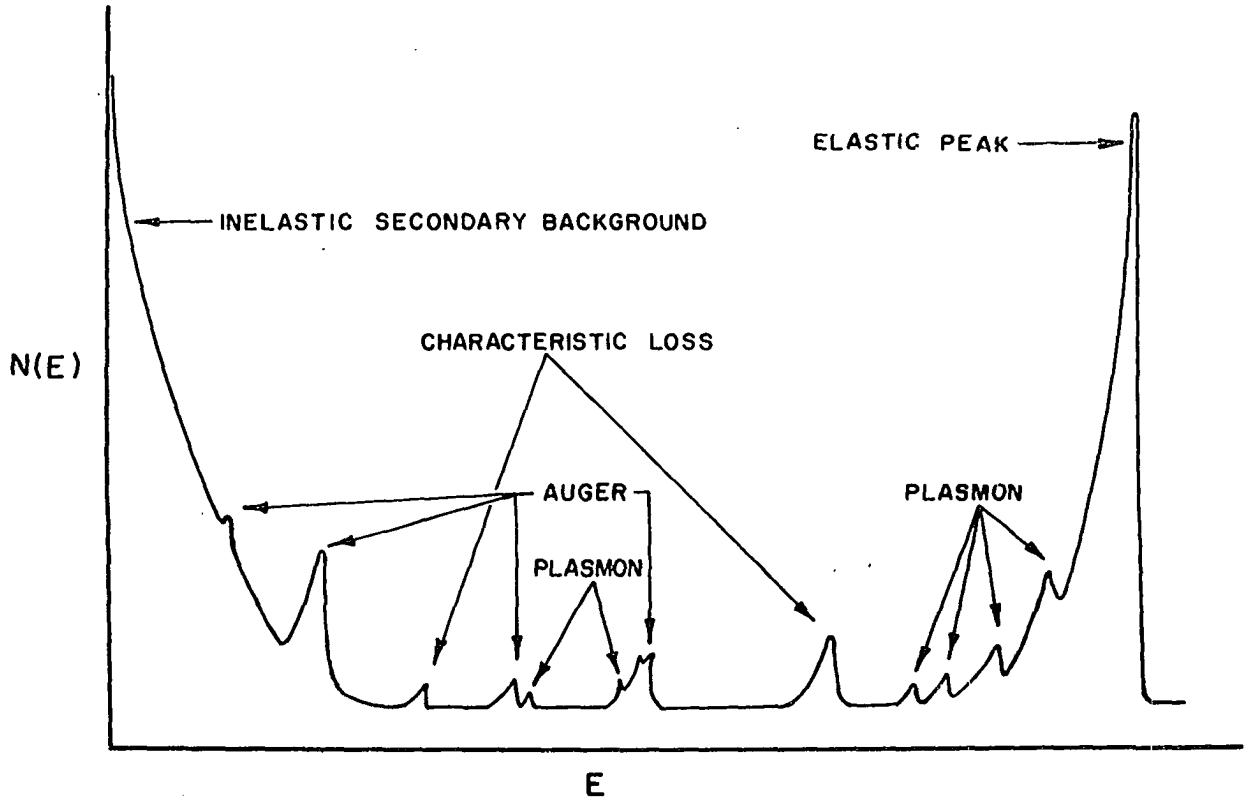

Figure 1. Electron-excited secondary electron spectrum.

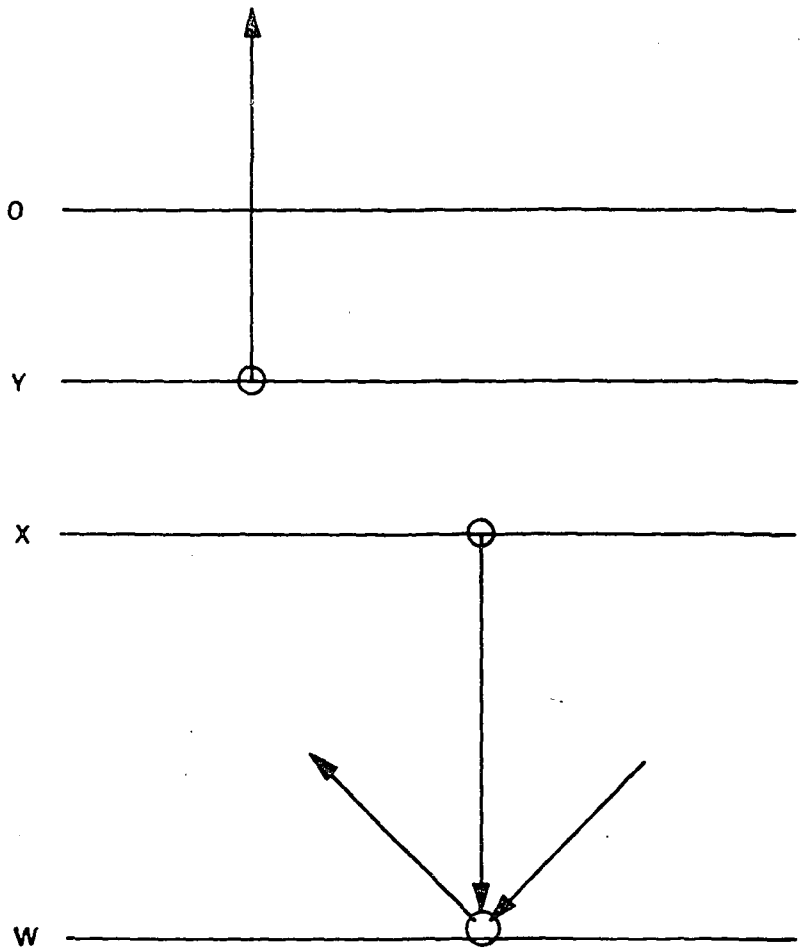

Figure 2. Auger process. Pictured is a general WXY transition with resultant kinetic energy $E_W-E_X-E_Y$

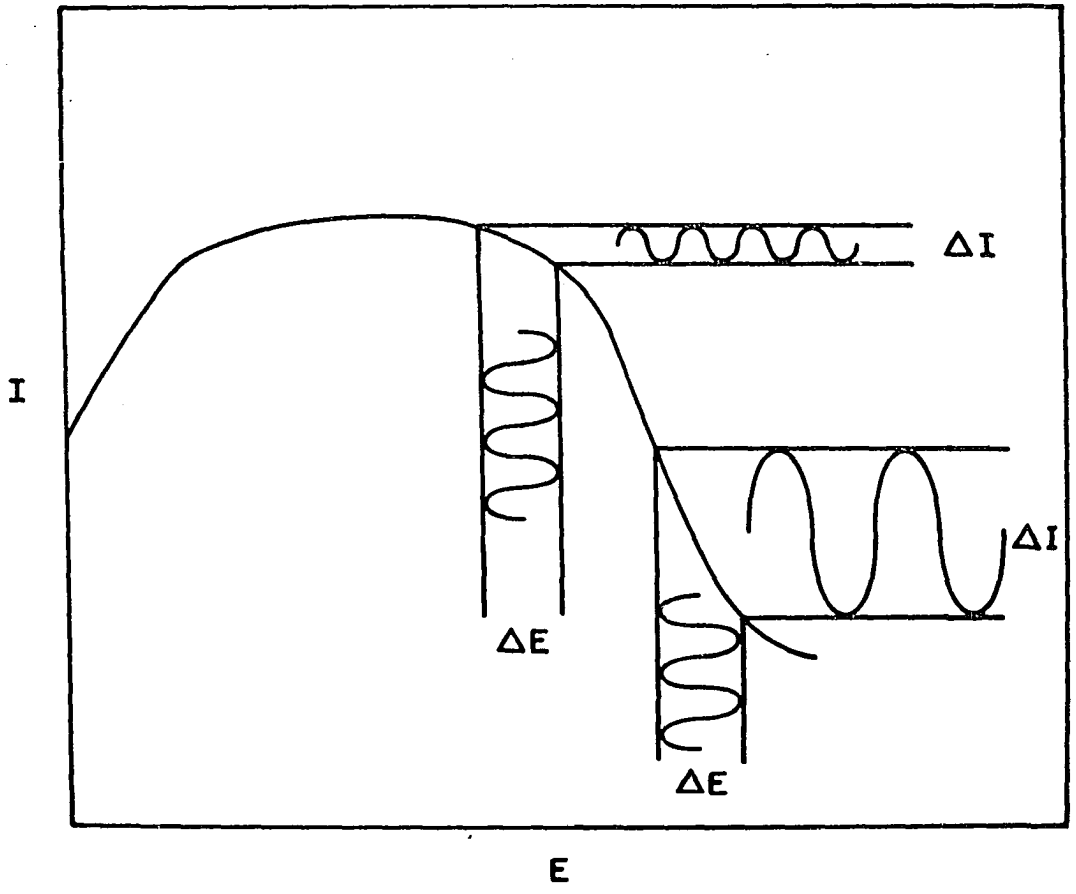

Figure 3. Electronic differentiation. An applied sinusoidal voltage ΔE produces ΔI.

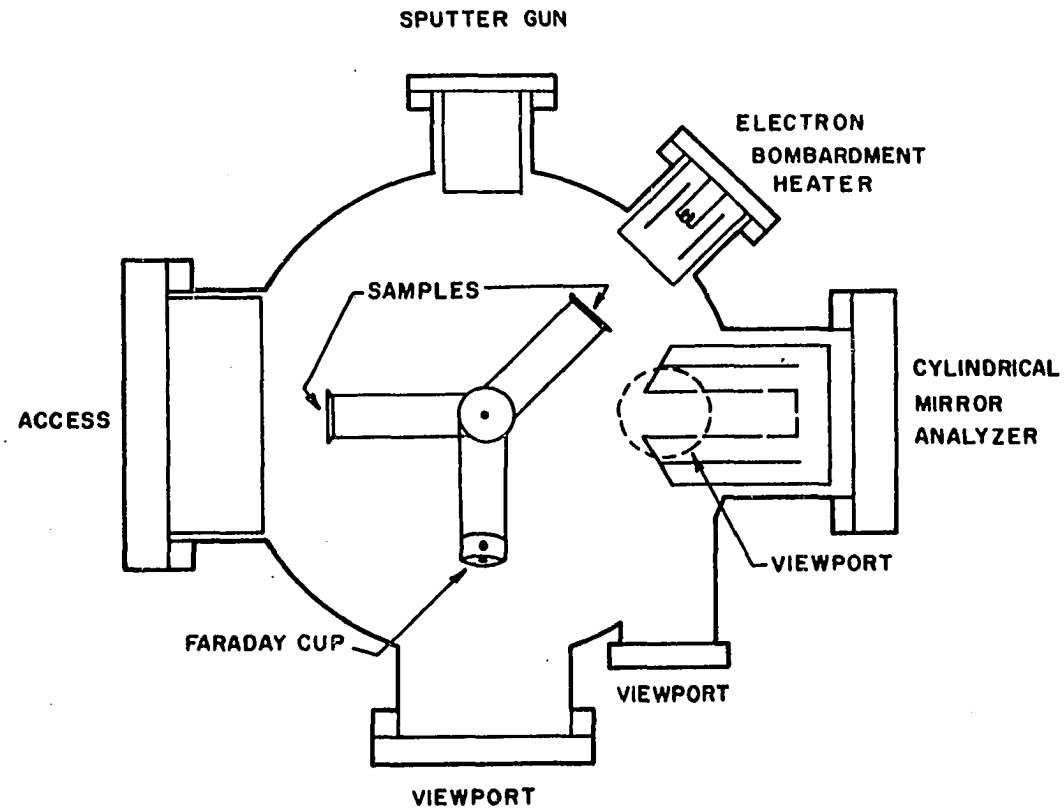

Figure 4. Schematic of the experimental arrangement (top view).

A plot of current collected vs. energy yields the secondary electron spectrum of Fig. 1. Unfortunately, Auger peaks are usually difficult to distinguish from the background. To reduce this problem the emission spectrum is differentiated electronically[10-13]. The method is schematically represented in Fig. 3. A small sinusoidal voltage ΔE is applied to the d.c. deflecting voltage. A phase-sensitive detector is referenced so as to discriminate the resulting change in current $\Delta N(E)$. The consequent $\Delta N(E)/\Delta E$ vs. E curve greatly reduces the continuous and slowly varying background while enhancing the Auger spectrum. The differentiated Auger peaks (Fig. 6) exhibit both positive and negative excursions--positive and negative $N(E)/\Delta E$. The minimum of the differentiated peak is taken as the Auger energy.

Characteristic Auger peaks result from electrons emitted in the first few monolayers[14-16], and sensitivity to surface species can therefore be enhanced using grazing incidence excitation. Because AES is a surface tool, ultrahigh vacuum is required to maintain an atomically clean sample surface for reasonable experimental times.

EQUIPMENT

Necessary instrumentation for Auger spectroscopy includes an excitation source, an electron energy analyzer, and the associated electronics. A phase-sensitive detector such as a lock-in amplifier for differentiation

of the electron spectrum is also required. An ultrahigh vacuum system and some means for obtaining clean surfaces complete the essential apparati.

The Auger and auxiliary equipment used in these studies were housed in an 11"-diameter, 13" long cylindrical stainless steel chamber. Rough vacuum was obtained by a cryosorption pump; ultrahigh vacuum was reached using 200 liter-per-second (lps) sputter-ion pumping augmented by a 200 lps titanium sublimation pump. The system was capable of less than 2×10^{-10} torr as measured by a Bayard-Alpert ionization gauge.

Arrangement of experimental apparatus in the chamber is shown in Fig. 4. In addition to the cylindrical mirror analyzer the facilities include an electron gun and sputter bombardment gun for cleaning (see Appendix III). Not shown in the top view of Fig. 4 is the specimen manipulator (Fig. 5) which allows 360° rotation, linear travel both along and transverse the axis of rotation, and tilt of the rotation axis up to 9° from normal.

A gas inlet system was constructed to allow admission of several cleaning gasses. The inlet line was separately pumped in order to maintain gas purity. It was also convenient vacuum procedure to backfill the chamber with dry nitrogen through the inlet when cycling to atmosphere. Both pumpdown time and initial contamination of the sample were thereby reduced. The variable leak valve through

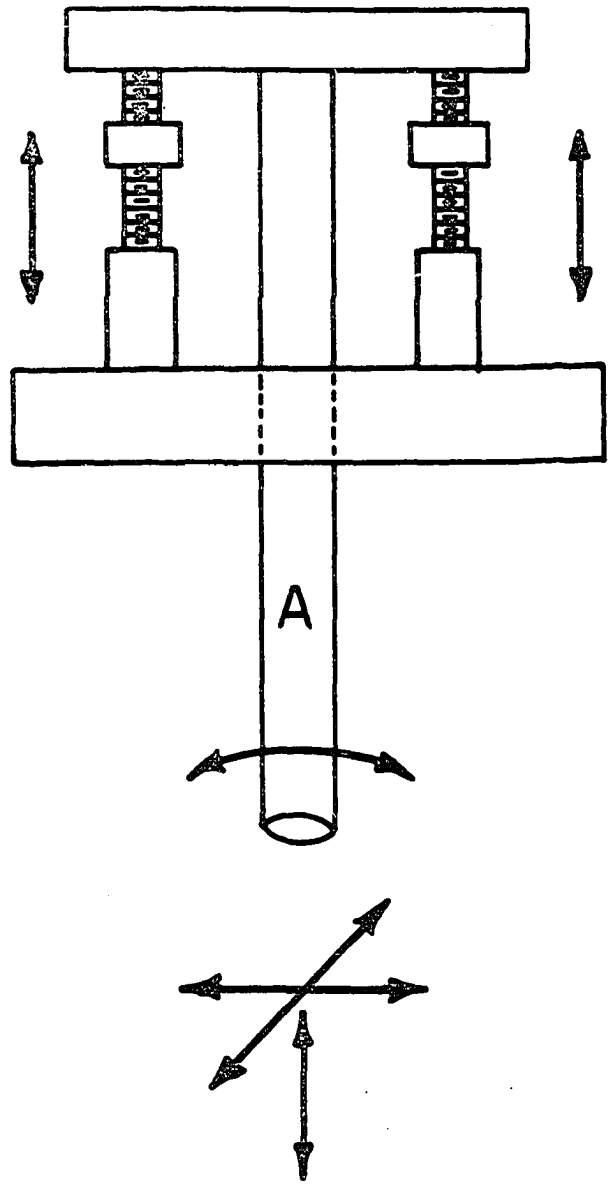

Figure 5. Specimen manipulator. Degrees of freedom shown are rotation and translation in three dimensions.

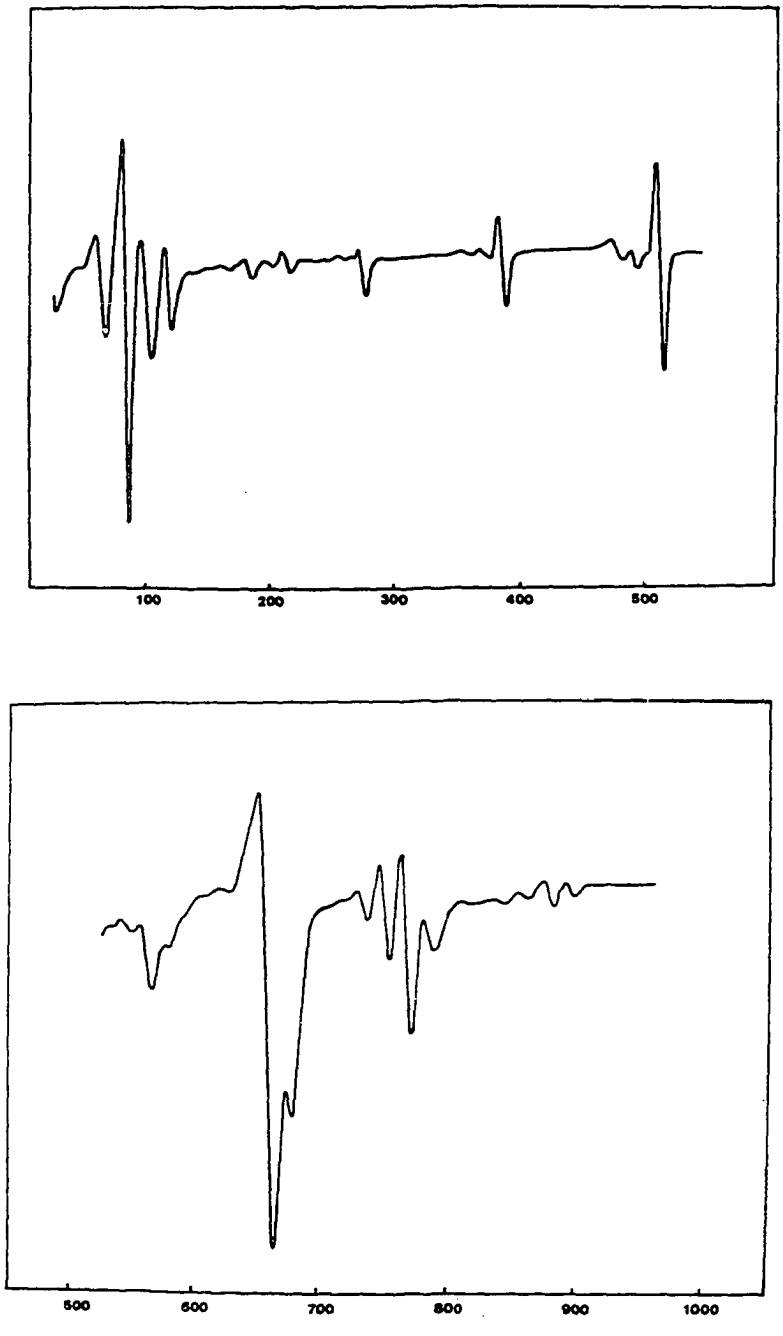

Figure 6. Cerium Auger spectrum. Horizontal axis is electron energy, eV. Sensitivity of higher range approximately 2.5 X that of the lower.

which gas entered the system features automatic pressure control and variable conductance 10^{-10} - 10^{2} standard cm^3/sec.

CHAPTER II

AES - LIGHT LANTHANIDE RARE EARTHS

The lighter lanthanide rare earths are the elements Ce, Pr, Nd, Sm, and Eu characterized by half-filling of the 4f orbitals. The artificial element Pm has not been studied, due to insufficient facilities for handling radioactive materials. The fourteen lanthanide rare earths share many properties; they are in general trivalent, chemically similar, strongly paramagnetic, and often exist as dissolved impurities in one another[17,18]. The lighter rare earths oxidize rapidly in air at room temperature, whereas the heavier elements are corrosion resistant. Because the different oxidation characteristics indicate probable distinction in Auger spectra and certainly in handling and cleaning procedures, the lighter and heavier elements were studied separately.

In this investigation it was purposed to obtain clean Auger spectra of the lighter rare earth elements. Unfortunately, not all contamination could be removed from the specimens, but the spectra obtained are thought to be representative of the clean surface. Secondly, it was hoped that because of the very similar overall electronic structure,

Auger peak intensities might be used to determine the density changes of the valence 4f orbitals with atomic number.

EXPERIMENT

The rapid oxidation of the samples necessitated several handling precautions. Specimens were received incased in heavy oil or under plastic seal. Inorganic solvents standard to vacuum procedure[19] were used in an inert atmosphere to remove these coatings. The samples were transferred under inert gas to the system and mounted. The chamber, which had been backfilled with dry N_2, was evacuated. A 200°C overnight bakeout followed which produced base pressures from $5 \cdot 10^{-10}$ to $5 \cdot 10^{-9}$ torr, depending on sample and peculiarities of the system.

Several in vacuo cleaning techniques were tried. Since oxygen was the principal evident contaminant, hydrogen reduction was attempted. The gas inlet system admitted H_2 to 10^{-4} torr. The sample was heated by electron bombardment to 400-1200°C for time periods of 15 min. to 3 hr. Little improvement was observed in Auger spectra subsequent to these procedures. It was not unusual for the carbon peak to increase while the O peak remained undiminished.

Alternating between simple e.b. heating and argon ion sputtering produced improvements in the Auger spectra. Sputtering was normally conducted at $5 \cdot 10^{-5}$ - $1 \cdot 10^{-4}$ torr as

described below. In this ambient, as in the hydrogen gas, difficulties were encountered with the electron beam heater gun due to electrical discharge and breakdown. It is assumed that the chief causes of these failures were vaporization of the sample onto the gun insulators and localized higher pressure regions in the vicinity of the gun and sample surface. For proper focusing the gun-sample distance was 1-3 cm, and gas evolution from the specimen surface was likely responsible for an observed gaseous blue discharge in the electron gun.

Of the methods attempted long-term argon sputtering produced the best results. Sputter times extended from one to four and a half days (for Europium), averaging thirty hours. In general the decrease in observed contamination appeared to be exponential, but since interruption of the sputter process to collect Auger spectra allowed recontamination, the exponential relationship is not confirmed. Sputtering was conducted under the following conditions: pressure - $5 \cdot 10^{-5}$ - 10^{-4} torr argon, accelerating voltage--400v, ion current density--approximately 10^{-5} $\frac{\text{amp}}{\text{cm}^2}$. The calculated removal rate is about .1 monolayer/sec.

Atomically clean spectra of the lighter rare earth elements were not obtained. In view of the calculated removal rate and analyzed purity of the samples this is surprising. However, there are several possible explanations. First, the removal rate calculation, which is only

a rough approximation, may be greatly erroneous. However, the average sputter time length surely resulted in the removal of several monolayers and therefore the removal of the region explored in the initial Auger spectrum. Since the surface analyzed after sputtering was entirely fresh, other causes for residual contamination are indicated. It is possible that a very thick oxide was formed on the sample, but in this case one would not expect to observe an exponential Oxygen intensity decrease until the oxides were nearly removed. A more likely cause is contamination to the sample during manufacture, shipping, handling, and vacuum preparation. Residual contamination thus represents base impurity levels in the specimen. Additionally, there is recontamination from the vacuum ambient. Assuming a unity sticking coefficient approximately one hour at 10^{-9} torr is required to form one monolayer on an atomically clean surface. Thus a base pressure of $5 \cdot 10^{-9}$ torr allows experimental times of about twelve minutes. Considerable recontamination occurs even during a normal two to four-minute spectrum, as well as that which accumulates during the set-up procedure. Lower base pressures obviously lessen the difficulty, but even at 10^{-9} torr times necessary for recording spectra assure a contamination build-up.

The principal impurity of the lighter lanthanide rare earths is oxygen. None of the cleaning treatments described above succeeded in reducing the oxygen 513 eV

Auger intensity much below one-half that of the major rare earth Auger peak. For the highly reactive elements Sm and Eu even this modest criterion was not attained. However, the intensity relationships and energies of the rare earth Auger peaks were in all cases apparently stabilized at contamination levels above those at which final spectra data were taken. While chemical effect on the Auger spectrum for oxygen bonding cannot be unambiguously established, it seems to be small. It is therefore assumed that the final results correspond to clean Auger spectra.

Minor amounts of carbon and nitrogen were also observed. Contamination levels were about ten per cent or less than that of oxygen as measured by Auger intensity. Sulphur was often found on samples prior to cleaning but was easily removed and did not reappear in the spectra. After sputtering a very small argon peak, due to imbedded Ar atoms, appeared. No other traceable contamination was present.

RESULTS

Spectra for the lighter rare earths are shown in Figs. 6-10. A summary of the spectra with semiquantitative intensity descriptions and transition identification is presented in Table 1.

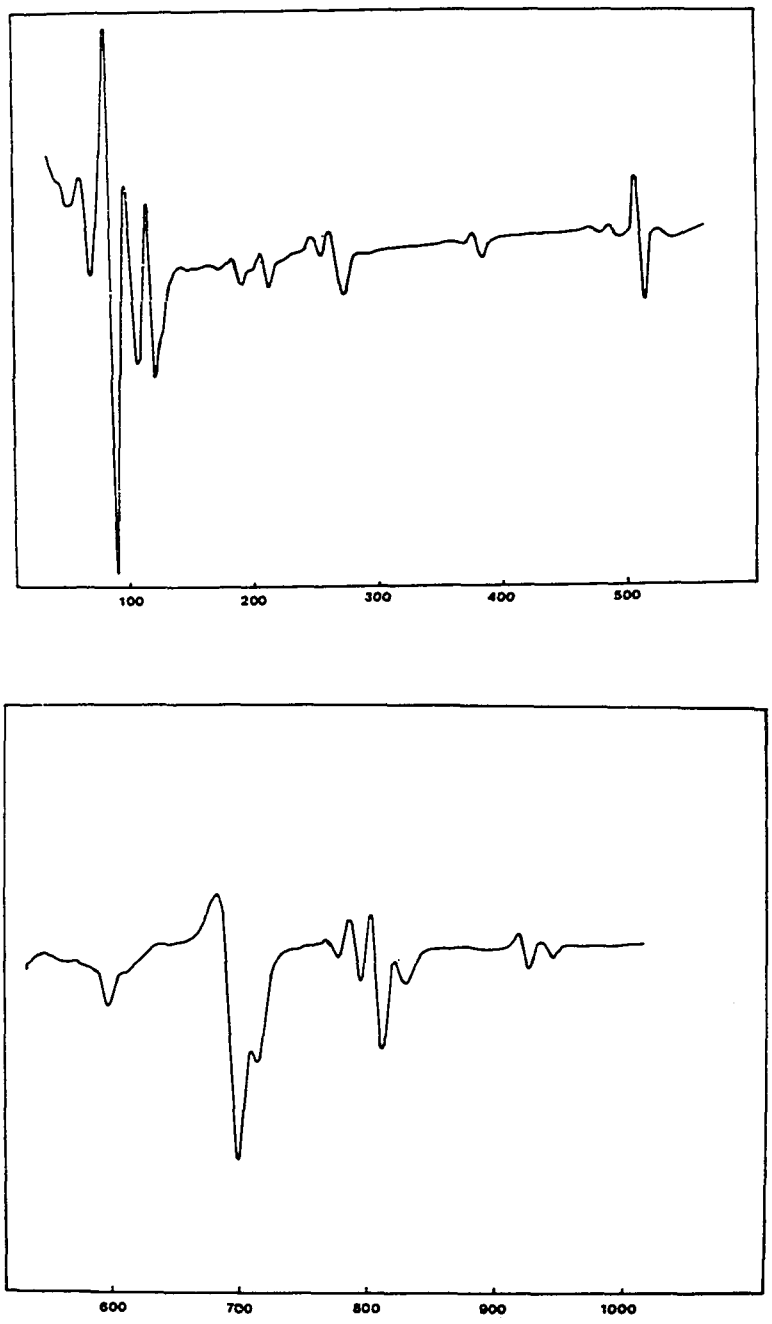

Figure 7. Praseodynium Auger Spectrum. Horizontal axis is electron energy, eV. Sensitivity of higher range is approximately 2.5 X that of the lower.

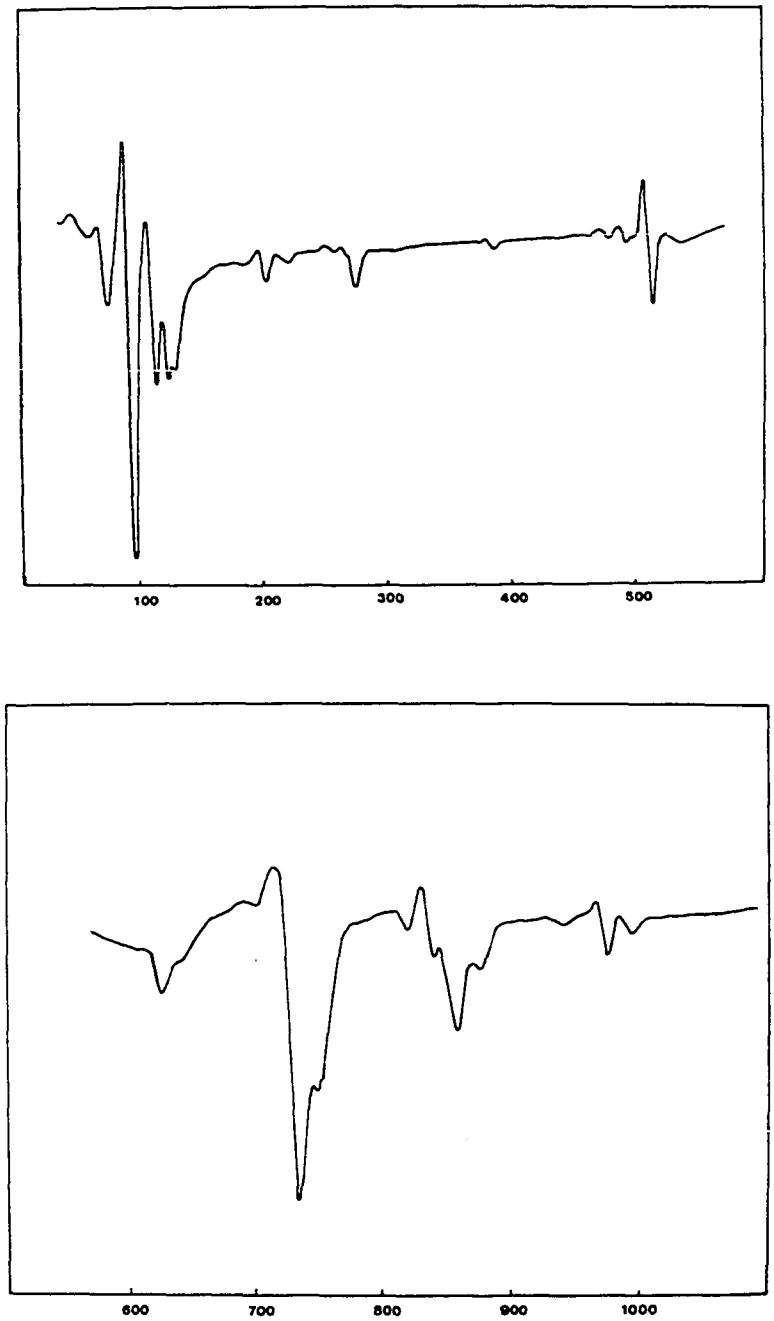

Figure 8. Neodymium Auger Spectrum. Horizontal axis is electron energy, eV. Sensitivity of higher range is approximately 2.5 X that of the lower.

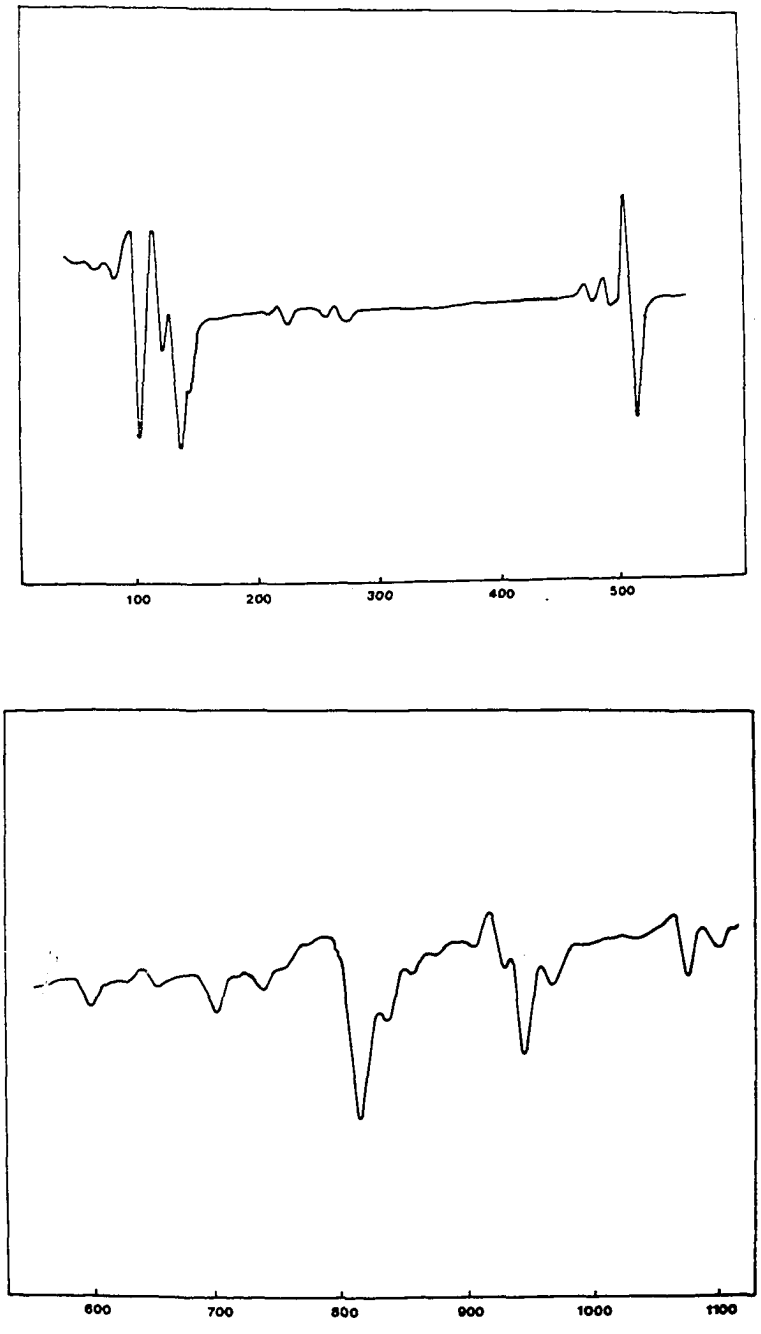

Figure 9. Samarium Auger Spectrum. Horizontal axis is electron energy, eV. Sensitivity of higher range is approximately 5.5 X that of the lower.

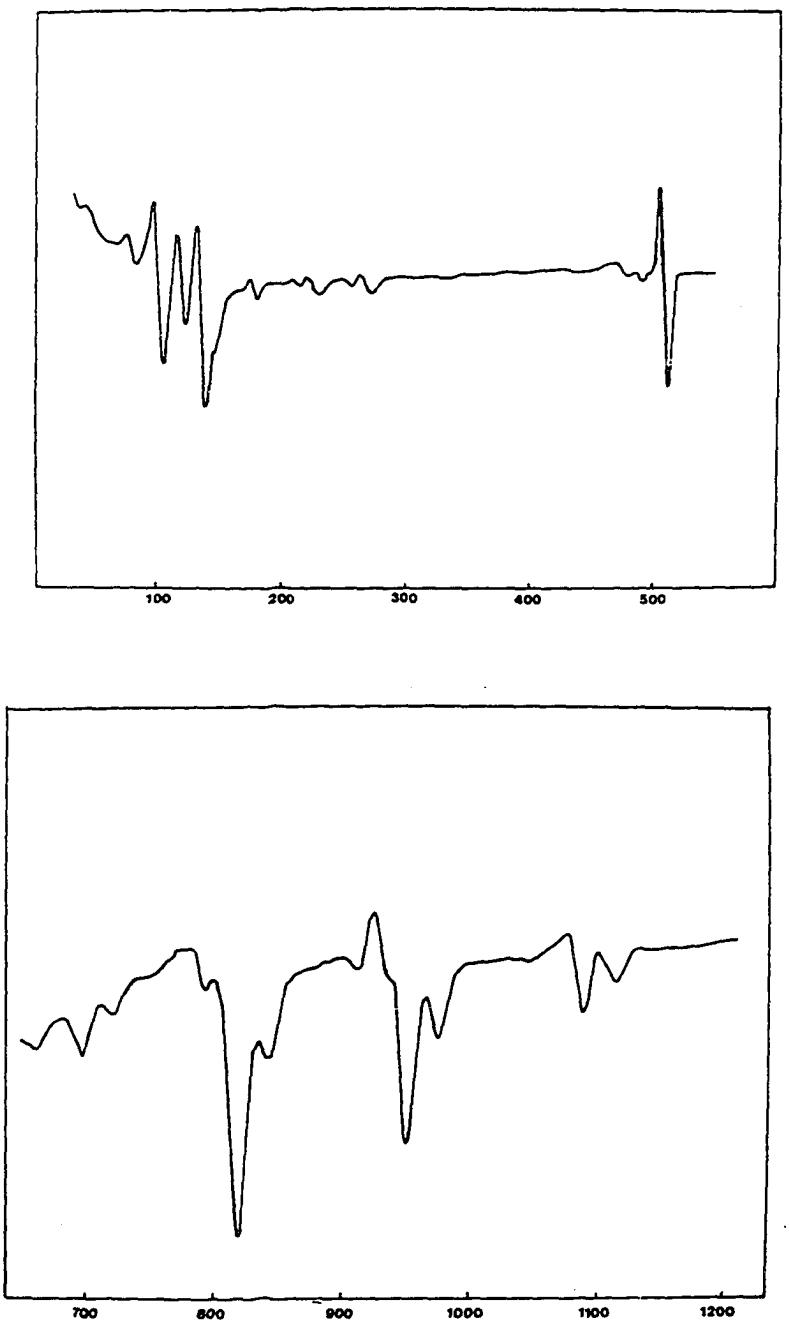

Figure 10. Europium Auger Spectrum. Horizontal axis is electron energy, eV. Sensitivity of higher range is approximately 5.5 X that of the lower.

DISCUSSION

The Auger transitions listed in Table 1 have been identified using X-ray notation[21] for atomic energy levels. While in the first approximation an Auger transition can be pictured as a WXY process, a more careful examination suggests several necessary modifications. It was found that for the lighter rare earths neither the simple calculation nor the usual modifications account for observed Auger energies. The assigned transition levels are thus extensions of the X-ray designations.

The difficulty becomes immediately apparent in the case of Ce, for which an Auger peak occurs at 121 eV. Threshold techniques determined the initial ionization to be less than 200 eV. Of the four energy levels listed in the atomic X-ray tables of Bearden and Burr[22], only the N_4 is in the proper energy range to initiate the Auger transition. But the N_4 is listed as 110 ± 0.6 eV - the maximum possible Auger energy for an N_4XY transition. It has been suggested[23] that higher energy satellites of Auger peaks represent transitions from once--or multiply--ionized atoms or plasmon gains, but peak magnitudes and energy separation between the 121 eV and the next lower 105 eV peak argue against either of these explanations.

It was observed from the discrete loss spectra (Chapter IV) that the N_4 level was 122 eV rather than 110 eV

Table 1

Auger energies (eV) for the lighter rare earths. Semiquantitative intensity descriptions are very strong (VS), strong (S), medium (M), weak (W), and very weak (VW).

	Ce	Pr	Nd	Sm	Eu
$N_4O_1O_2$	67 S	71 M	74 S	81 M	84 M
$N_4N_4O_1$	89 VS	91 VS	94 VS	104 VS	106 S
$N_4N_6O_2$	105 S	107 S	111 S	121 S	124 S
$N_5N_6N_6$	121 S	123 S	125 S	136 VS	140 VS
$N_5N_6N_6$		127 S	129 S	142 S	146 S
$N_3N_6O_2$	185 M	193 M	202 M	222 M	230 M
$M_5N_1N_4$			536 W	599 M	631 W
Unidentified				651 W	704 W
$M_5N_1O_1$	565 M	597 M	626 M	701 M	735 M
$M_5N_1O_2$	579 W	612 W	642 W	717 W	758 W
$M_5N_4N_4$	653 VS	699 VS	734 VS	814 VS	858 VS
$M_4N_4N_4$	676 S	714 S	749 S	835 S	881 M
$M_5N_4O_1$	735 W	777 W	818 W	904 W	
$M_5N_4O_2$	752 M	794 M	839 M	927 M	950 W
$M_5N_4N_6$	769 S	811 S	858 S	943 S	984 S
$M_4N_4N_6$	787 M	830 M	877 M	965 M	1009 M
$M_5N_6N_6$	879 W	926 W	975 M	1074 M	1125 M
$M_4N_6N_6$	896 W	945 W	994 W	1098 W	1152 M

for surface atoms excited by 2-3 keV electrons. Simple subtraction calculations using this 122 eV value and those from X-ray tables for $N_{6,7}$, O_1, and $O_{2,3}$ levels produced excellent agreement between empirical and calculated Auger transitions of the type $N_{4,5}$ XX, where X = $N_{6,7}$,O_1 or $O_{2,3}$.

One other feature of the Auger spectra not expected from X-ray data was the doublet $N_{4,5}N_{6,7}N_{6,7}$ splitting for elements Pr, Nd, Sm, and Eu. Again the explanation lies in the differences at the $N_{4,5}$ level between X-ray and electron excited loss data. The latter display a splitting of the N_4 and N_5 levels which are degenerate according to X-ray findings. The separate N_4, N_5 account for the observed doublet Auger transitions.

There are many objections to the quantitative use of differential Auger peak intensities between peaks. Overlap of adjacent peaks, especially of the low energy tail, inexact correlation between N(E) peak intensity and maximum slope, backscattered contributions depending on Auger energy, correlation between incident energy and Auger intensity, and additive background and loss-gain effects are but a few. It is almost impossible, however, to avoid a natural temptation to attempt quantitative use of Auger intensities, particularly among peaks in the same energy range. Furthermore, there is evidence[14,16,24-28] that such information is indicative, if not conclusive. For the rare earth series the growth of the last peak ($N_{4,5}$

$N_{6,7}N_{6,7}$) of the major group with increasing atomic number at the expense of others of the same group, particularly the second ($N_4N_6O_1$), leads to quantitative speculation. Simply, it appears that the filling of the 4f ($N_{6,7}$) orbital is reflected in the Auger intensity most connected with that level. In turn this indicates that proper identification has been made of the empirical data. Furthermore, it implies that the Auger intensities of the major peak group are results of a simple numeric probability of transition. Unfortunately, scale standardization is presently impossible between samples due to an absence of any internal criterion and large effects on intensity produced by contamination and sample position. Therefore the description remains strictly semiquantitative. A plot of the general intensity trends vs. atomic number appears in Fig. 11.

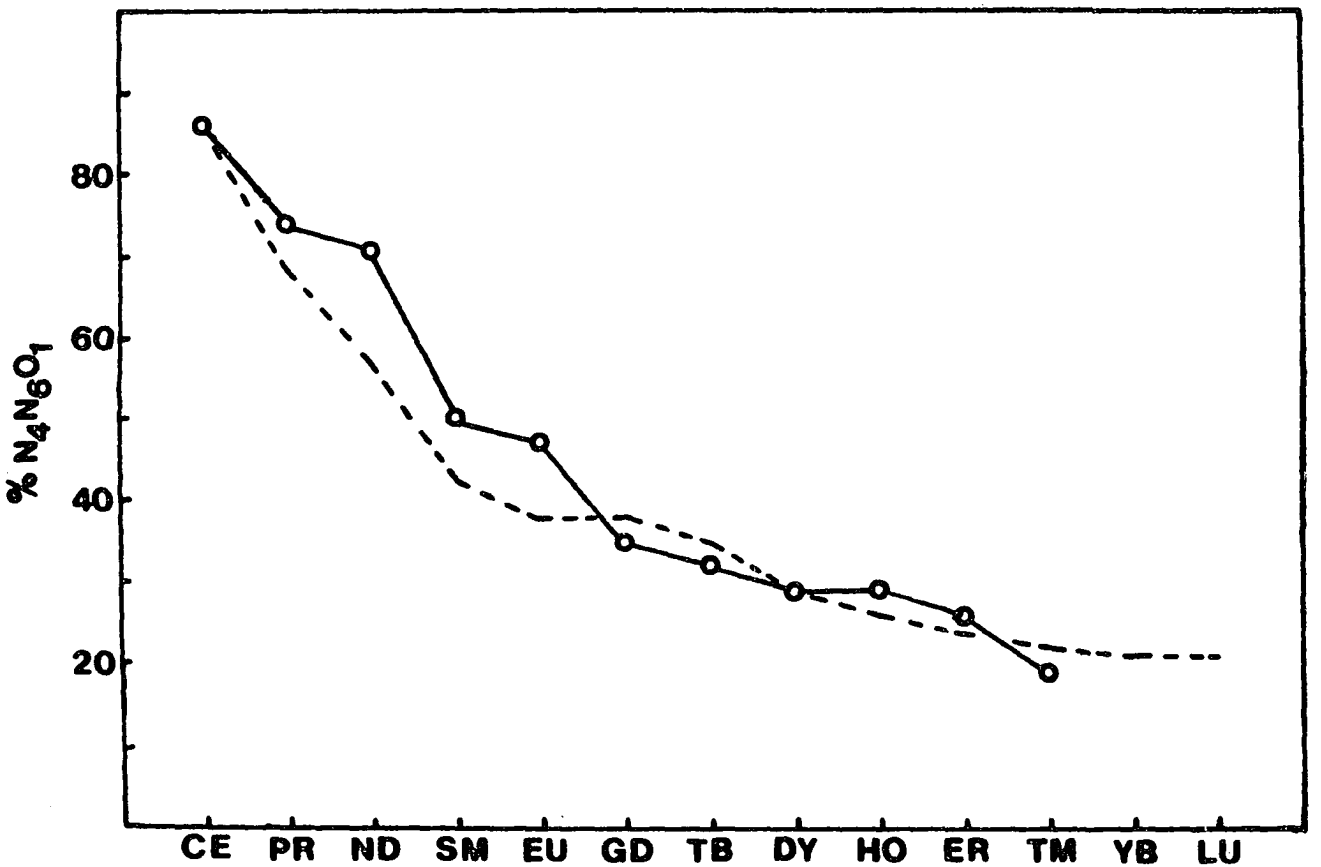

Figure 11. Percentage ratio of the peak to peak intensities. $N_4N_6O_1/N_4N_6O_1 + N_4N_6N_6$. Dashed line is the theoretical intensity based upon the electron ratios of the N_6 (4f) and O_1 (5s) levels times the constant 1.72.

CHAPTER III

AES - HEAVY LANTHANIDE RARE EARTHS

INTRODUCTION

In this study Auger spectra for the heavy rare earths --Gd, Tb, Dy, Ho, Er, Tm, Yb, and Lu--have been determined. As a result of the 4f subshell filling sequence the different atoms appear electronically quite similar. The heavier of the rare earths share a resistance to corrosion, as well as many other chemical similarities. It was expected that considerable correspondence would exist among the Auger spectra for the rare earths, as previous work[20] has shown similarities between the Auger spectra for the transition metals.

EXPERIMENT

After a standard degreasing process, each high purity rare earth sample was mounted in the vacuum chamber. A twelve hour, 200° bakeout usually produced a system pressure about 5×10^{-10} torr. High purity argon was then admitted to sputtering pressure of 10^{-4} torr. Lengthy sputtering by a 0.5 cm diameter 20 ma beam was required for each of the elements in order to obtain spectra

representative of a clean surface. Mean sputter time was sixteen hours at 10^{-4} torr argon.

Data was taken under the following conditions: (1) active gas pressure--less than 10^{-9} torr, (2) 2 Kv accelerating voltage, (3) beam current--65 μa, (4) modulation amplitude--2 v peak to peak. An experimental run included the Auger spectrum from 100-200 eV and the characteristic loss spectra for various primary beam voltages.

Carbon and oxygen were found to be the principal contaminants. As mentioned above long sputter times were necessary to reduce the C (275 eV) and O (513 eV) peaks to negligible intensities. Dirty samples of the rare earths also exhibited the presence of iron and nickel (probably from the stainless steel sample holder), and the N (385 eV) peak was observed. Sulphur, present on the specimens before cleaning, was easily removed by the sputter process. After sputtering the Ar (216 eV) peak, due to imbedded Ar, appeared in the spectrum.

RESULTS AND CONCLUSIONS

Table 2 lists the energy of the Auger peaks for each element. The values have been labeled by the corresponding X-ray energy level designations. Included are semiquantitative descriptions of the peak intensities. The Auger spectra obtained for each element are shown in Figs. 12-19.

Table 2

Auger energies (eV) for the heavier rare earths. Semiquantitative intensity descriptions are very strong (VS), strong (S), medium (M), weak (W), and very weak (VW).

	Gd	Tb	Dy	Ho	Er	Tm	Yb	Lu
$N_4O_1O_2$	91 M	95 M	105 W	114 W				
$N_4N_6O_1$	111 S	117 S	120 S	129 S	135 M	143 M		153 W
$N_4O_6O_2$	131 M		134 W	144 M	151 M	157 S	162 M	161 M
$N_5N_6N_6$	142 VS	149 VS	146 S	156 VS	161 VS	170 VS	172 VS	174 VS
$N_4N_6N_6$	142 VS	149 VS	155 VS	160 VS	166 VS	170 VS	177 VS	183 VS
$N_3N_6O_2$	240 M	251 M	257 M	266 M	285 M	296 S	309 M	321 M
$N_3N_6N_6$							326 M	334 M
$M_5N_1N_4$	658 W	689 W	720 VW	747 VW	780 VW	815 VW	846 VW	874 VW
Unidentified	728 VW	759 VW	794 VW	821 VW	862 VW	895 VW	931 VW	966 VW
$M_5N_1O_1$	765 M	799 M	833 W	871 VW	906 VW	944 VW	789 VW	1023 VW
$M_5N_1O_2$	793 W	828 W	865 VW	903 VW	939 VW	980 VW	1024 VW	1061 VW
$M_5N_4N_4$	895 S	933 S	976 M	1013 M	1054 M	1096 M	1140 M	1180 M

Table 2 (Continued)

	Gd	Tb	Dy	Ho	Er	Tm	Yb	Lu
$M_4N_4N_4$	920 M	958 M	1001 W	1043 W	1087 W	1129 W	1179 W	1225 W
$M_5N_4N_6$	1028 S	1075 S	1124 M	1172 M	1221 M	1269 M	1323 M	1370 M
$M_4N_4N_6$	1056 M	1106 M	1155 W	1207 W	1264 W	1300 W	1360 W	1411 W
$M_5N_6N_6$	1176 M	1222 M	1280 M	1334 M	1390 M	1446 M	1506 M	1560 M
$M_4N_6N_6$	1200 W	1252 M	1311 M	1370 M	1428 M	1490 W	1554 W	1611 W

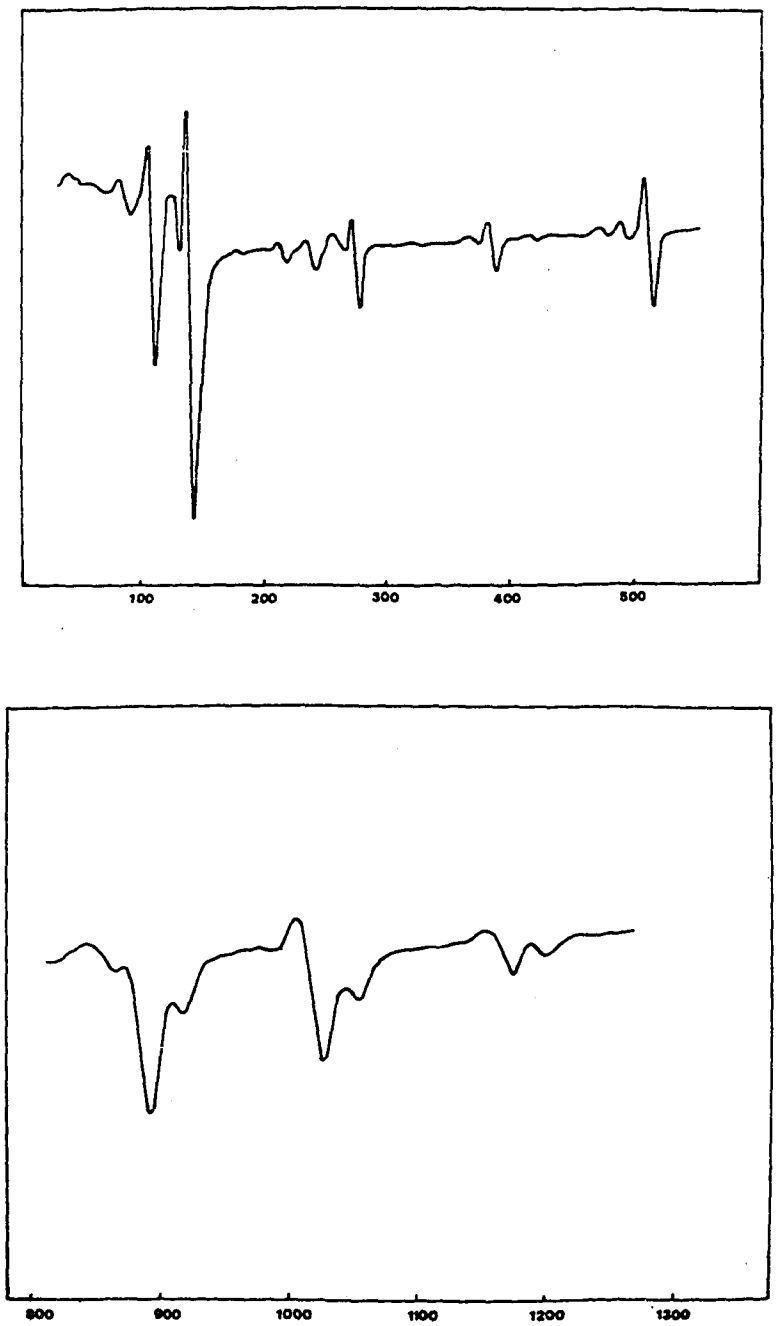

Figure 12. Gadolinium Auger Spectrum. Horizontal axis is electron energy, eV. Sensitivity of higher range is approximately 2X that of lower.

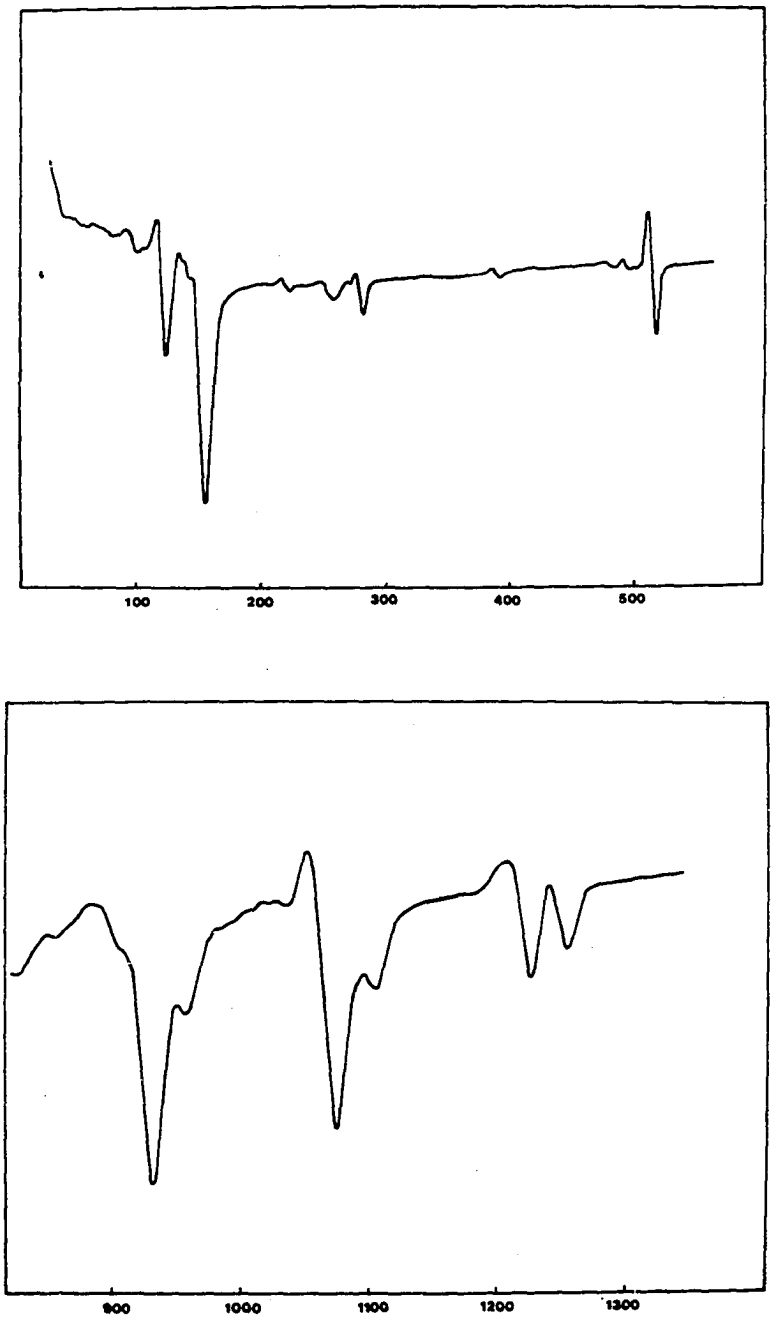

Figure 13. Terbium Auger spectrum. Horizontal axis is electron energy, eV. Sensitivity of higher range is approximately 5X that of lower.

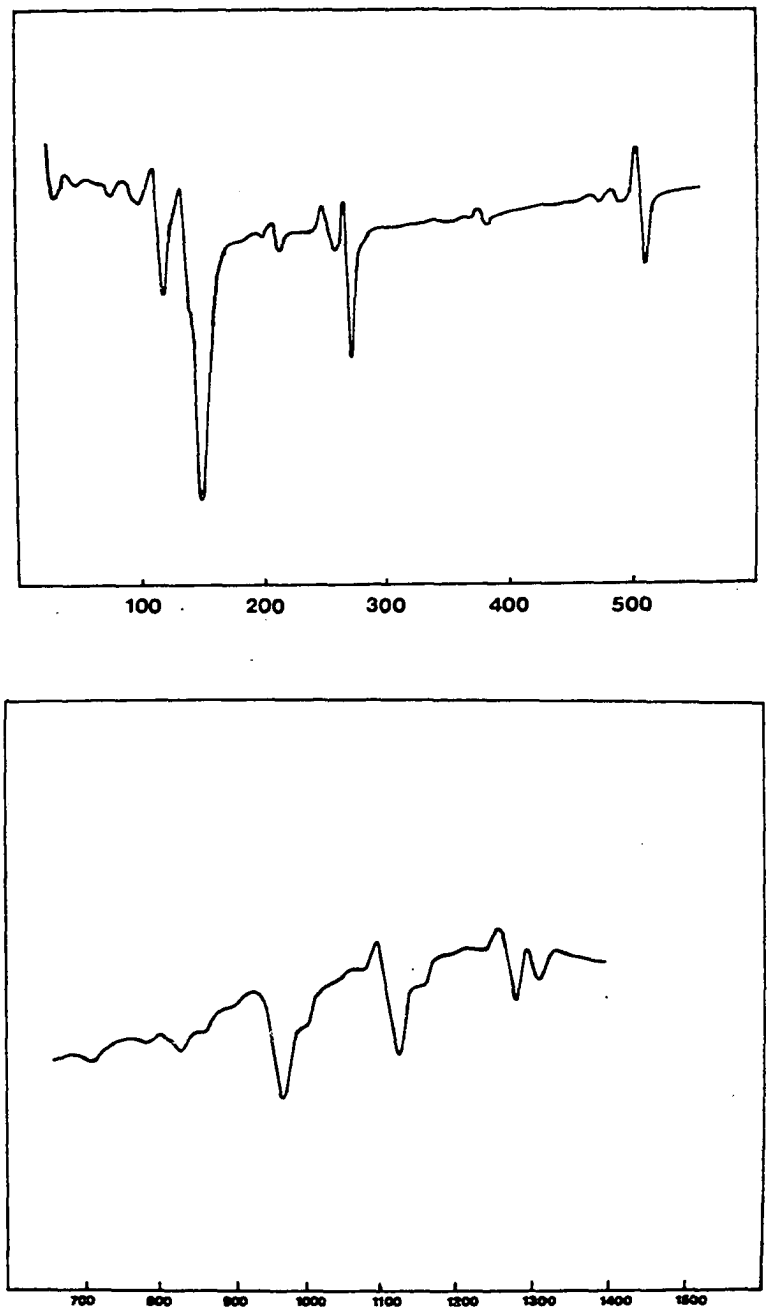

Figure 14. Dysprosium Auger Spectrum. Horizontal axis is electron energy, eV. Sensitivity of higher range is approximately 2X that of lower.

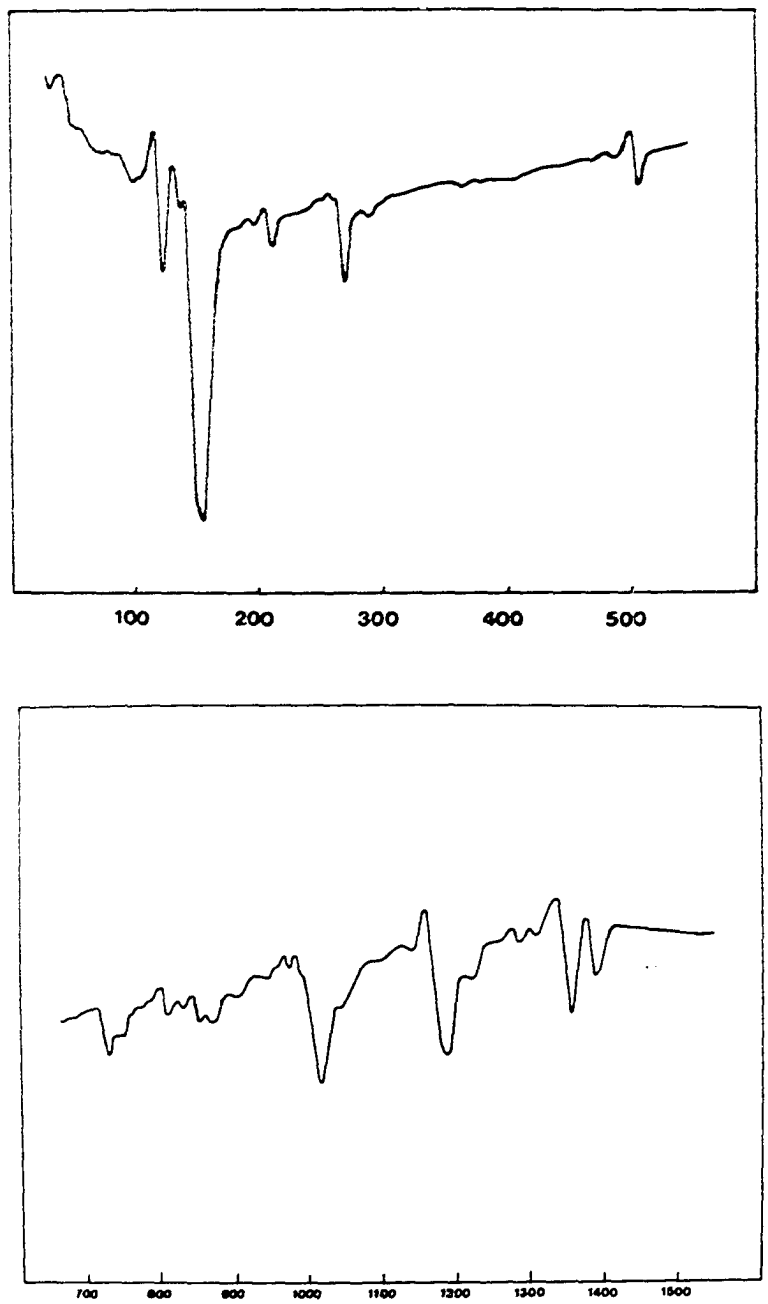

Figure 15. Holmium Auger spectrum. Horizontal axis is electron energy, eV. Sensitivity of higher range is approximately 2X that of lower.

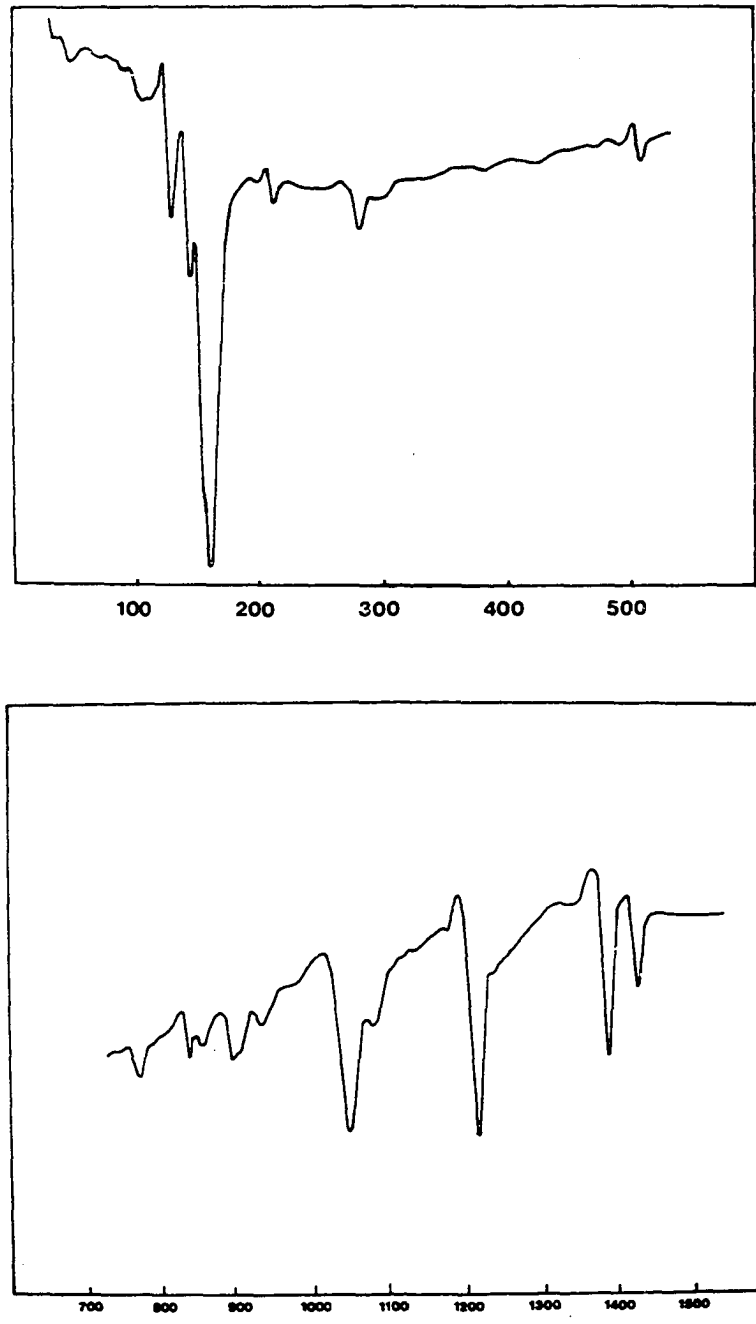

Figure 16. Erbium Auger spectrum. Horizontal axis is electron energy, eV. Sensitivity of higher range is approximately 5X that of lower.

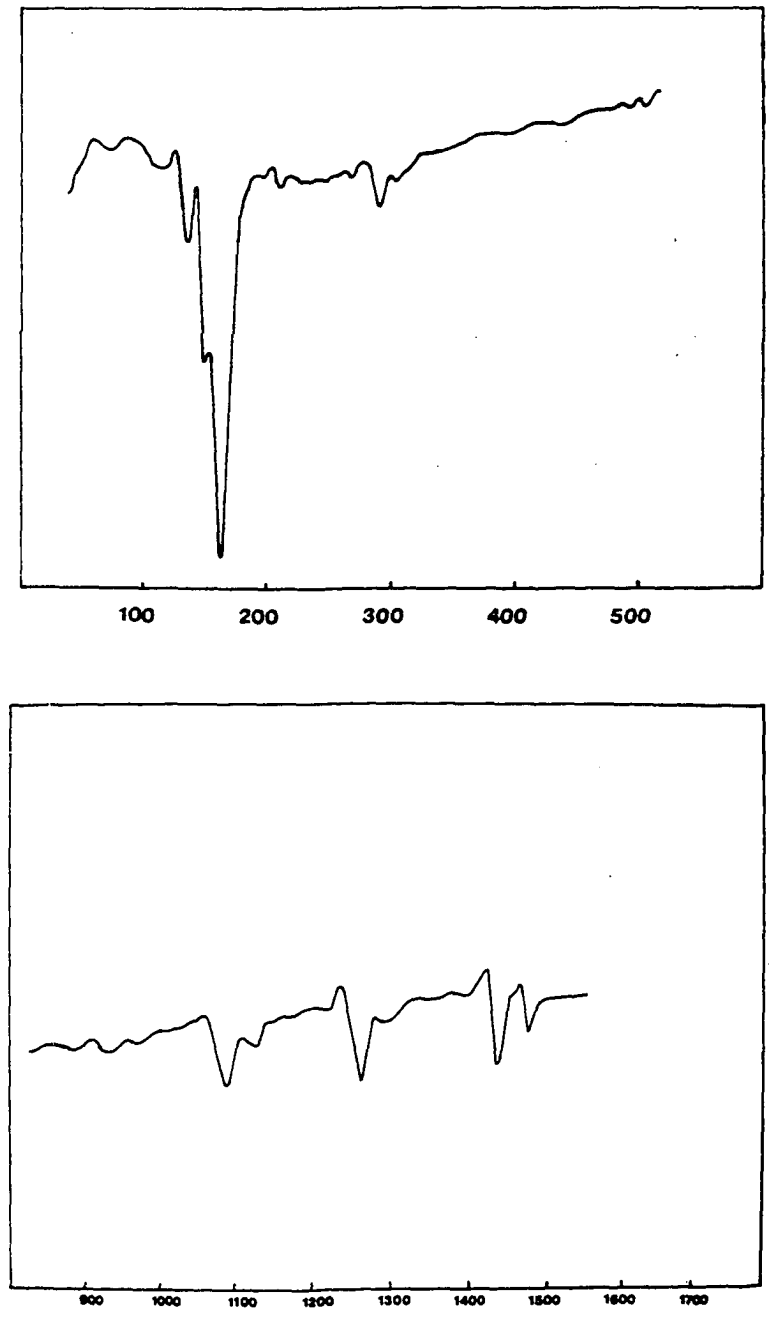

Figure 17. Thulium Auger spectrum. Horizontal axis is electron energy, eV. Sensitivity of higher range is approximately 2X that of lower.

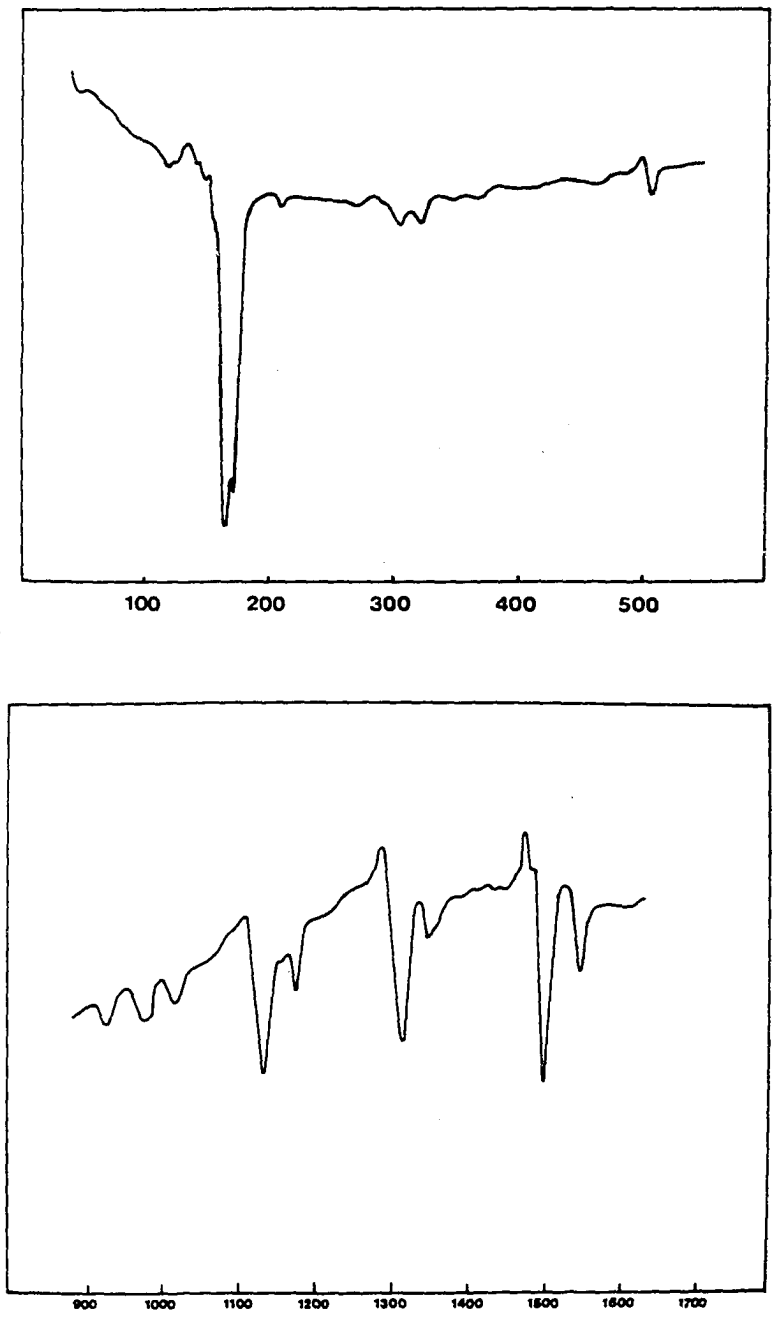

Figure 18. Ytterbium Auger spectrum. Horizontal axis is electron energy, eV. Sensitivity of higher range is approximately 5X that of lower.

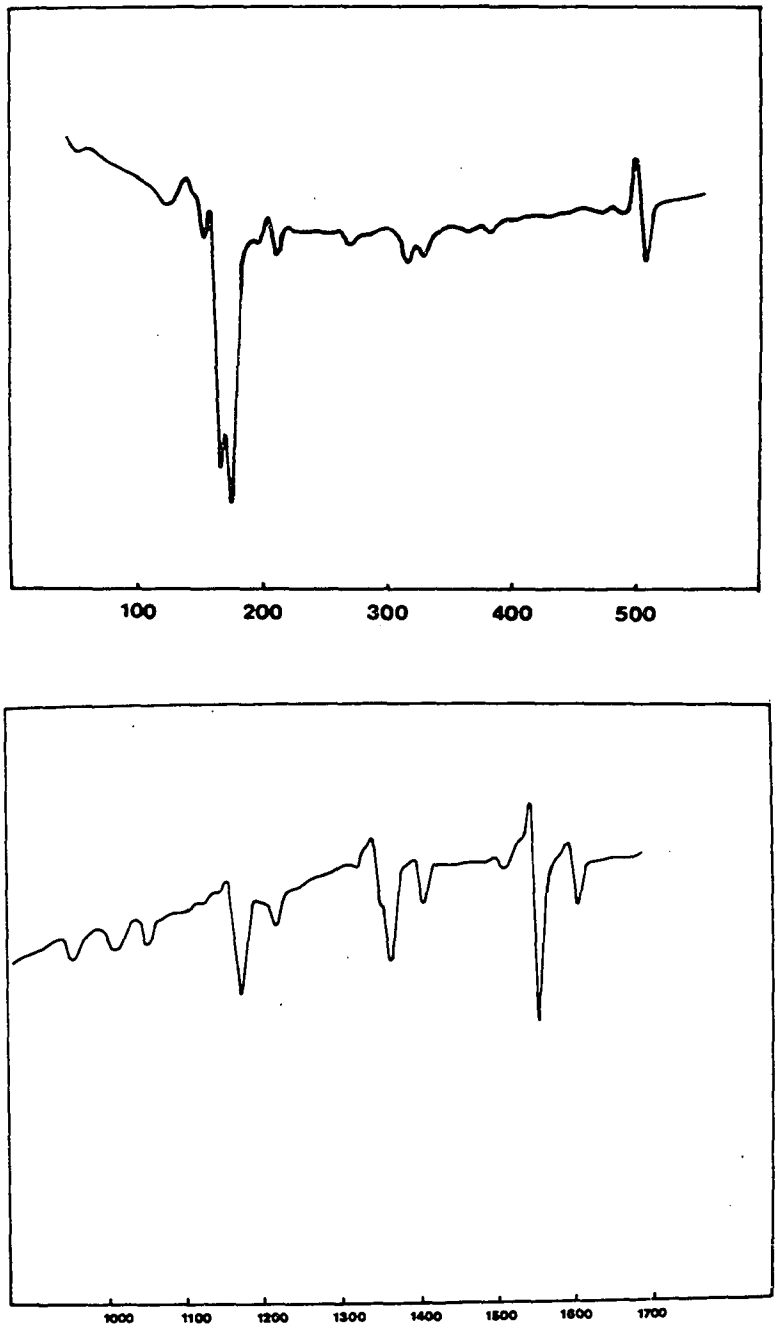

Figure 19. Lutetium Auger spectrum. Horizontal axis is electron energy, eV. Sensitivity of higher range is approximately 5X that of lower.

It can be seen from the table that Auger peak energies increase with increasing atomic number. This relationship corresponds qualitatively to the theoretical approximation using atomic energy levels, but is opposite to results for the period 6 transition series[29,30].

Many of the transitions, such as those for the N_1 and N_2 levels, are absent from this series of spectra. This is consistent with the absence of the corresponding characteristic loss peaks due to these levels. The transitions after initial ionization for the most part involve electrons having energies of 200 eV or less from vacuum level. The reason for the general exclusion of higher energy levels from the second and third steps of the Auger process is not clear. These two factors combine to limit the number of Auger peaks to only a few of the hundreds possible from energy considerations alone.

Of these elements only Tm appears to have degenerate N_4-N_5 levels. The other elements show the structure reported in Table 1 due to separate N_4 and N_5 energies. This is most noticeable for Yb and Lu (Figs. 18, 19). Some evidence of this same fine structure was found for the higher energy peaks involving the N_4 and N_5 transition, but results were not conclusive. This finding does not agree with atomic energy level data for Dy and Ho[22] which show a degenerate N_4-N_5 energy. Non-degenerate N_4 and N_5 levels for the surface sensitive Auger process suggest an electronic

structure for electron-excited surface atoms significantly different from that for the bulk, due to X-ray ionization.

From the above the following conclusions may be drawn:

(1) Auger spectra for the latter part of the rare earth series are strikingly similar. This similarity is not unexpected when the correlated chemical nature of the elements are considered.

(2) In general Auger peaks for these elements are within 200 eV of the initial ionization energy.

(3) The extent of initial ionization is not controlled solely by energy requirement.

CHAPTER IV

IONIZATION LOSS SPECTROSCOPY

X-ray atomic energy level tables, particularly those of Siegbahn et al[31] and Bearden and Burr[22], have been used to calculate Auger energies and thereby assign WXY transitions[29,30] to observe Auger peaks. Applicability of this technique has recently been questioned[13].

An obvious error is introduced by assuming that energy levels of the ionized atom during Auger transition remain unchanged from those of the neutral atom. The well-known modifications of Bergstrom and Hill[1] and Chung and Jenkins[2] attempt to correct this problem by viewing core ionization as a reduction in the effective screening of outer shell electrons from the nucleus. Bergstrom and Hill's effective binding energy is computed as

$$E'_Y(Z) = E_Y(Z) + \Delta Z(E_Y(Z+1) - E_Y(Z))$$

where $E'_Y(Z)$ is the perturbed binding energy of the Y level atomic number Z electron, $E_Y(Z)$ its unperturbed energy, $E_Y(Z+1)$ the Y level bonding energy for element Z+1, and ΔZ an empirical constant. The expression of Chung and Jenkins is similar, symmetrized to account for both WXY and WYX transitions.

Grant and Haas[32] have shown that carbon can be identified as to chemical state by its Auger spectrum. In their experiment carbon present in graphite form in CO-CO_2, or in TaC produced distinctive fine structure of the C Auger peak. These results are attributed to altered electronic structure of carbon in its different chemical combinations.

The reasonable assumption of disparity between the electronic structures of surface and bulk atoms has been used successfully in the work function calculations of Steiner and Gyftopoulos[33]. This suggests that Auger energies, the result of surface electronic transitions[14-16], are not adequately determined by reference to bulk atomic energy levels. The common X-ray measurements - absorption edge, X-ray flourescense, and photoelectric emission by high energy X-rays - employ far greater penetration and/or escape depths than those associated with low energy (1000 eV) Auger transitions. The X-ray atomic energy level tables may be regarded as appropriate for atoms in the bulk state but questionable when applied to surface atoms.

Haas, Grant, and Dooley[29], Aksela, Pessa, and Karras[34, 35] and Coad and Riviere[36], investigating the first transition series metals, have discovered doublet fine structure for each of the Auger transitions $L_3M_{2,3}V$, $L_3M_{2,3}M_{2,3}$, and $M_{2,3}VV$. Coad and Riviere attribute the doublet peaks to splitting of the $M_{2,3}$ level--listed as degenerate in the X-ray data of Bearden and Burr[22].

Because of the several questions raised concerning use of X-ray energy levels, the determination of energy levels at a surface under electron excitation is valuable. Fortunately, a simple method can be used to obtain necessary information. The secondary electron spectrum includes a background of inelastically scattered electrons, Auger peaks, the elastic peak, and loss peaks due to plasmon interactions and to ionizations of the target atom (Fig. 1). The last peaks are characteristic of the atomic energy levels. They have energy $E_I = E_P - E_W$, where E_I is the ionization loss peak energy, E_P the incident electron energy and E_W the energy of the initially ionized atomic energy level (Fig. 20). Atomic energy levels are equal to $E_P - E_I$ and can be determined using common Auger equipment and techniques.

Ionization loss peaks are easily distinguished from Auger transitions, since the former vary as the excitation energy, while the latter remain at constant energy--though not intensity[12,13,31]--as long as the primary energy is above threshold. Once E_W is generally established, E_I can be set conveniently by change in E_P. An example of ionization loss peaks is shown in Fig. 21. Some of the considerations involved can be seen as well. Naturally the energy E_I must not lie near or on Auger peaks. Since resolution for the cylindrical mirror analyzer is a constant 0.6%--i.e. contribution to peak width is linear[5-9,38]--

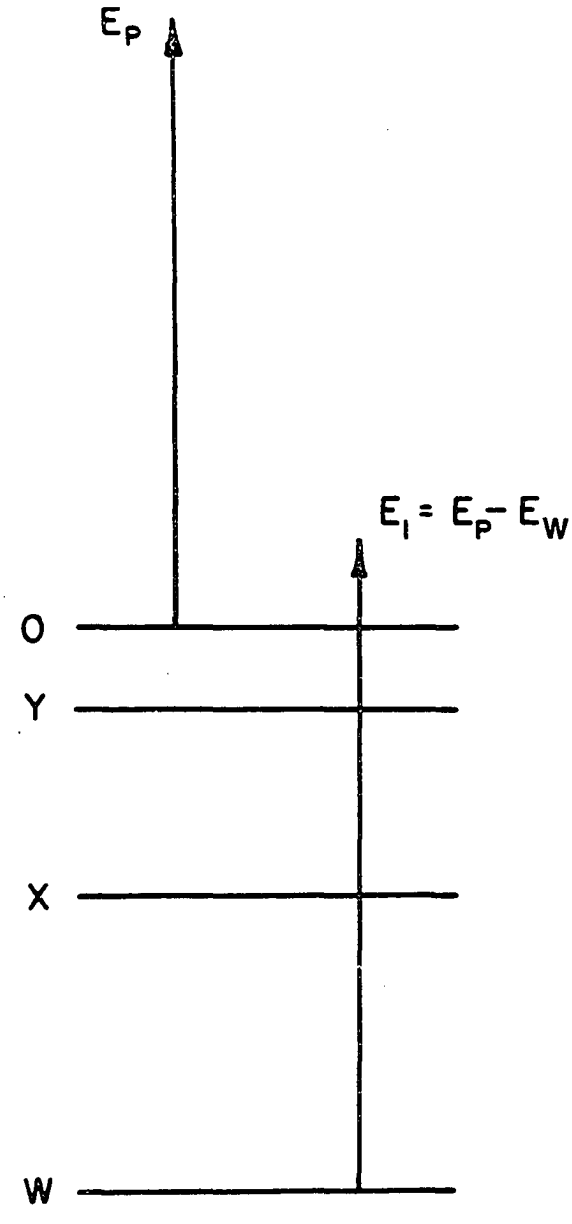

Figure 20. Ionization loss energy diagram.

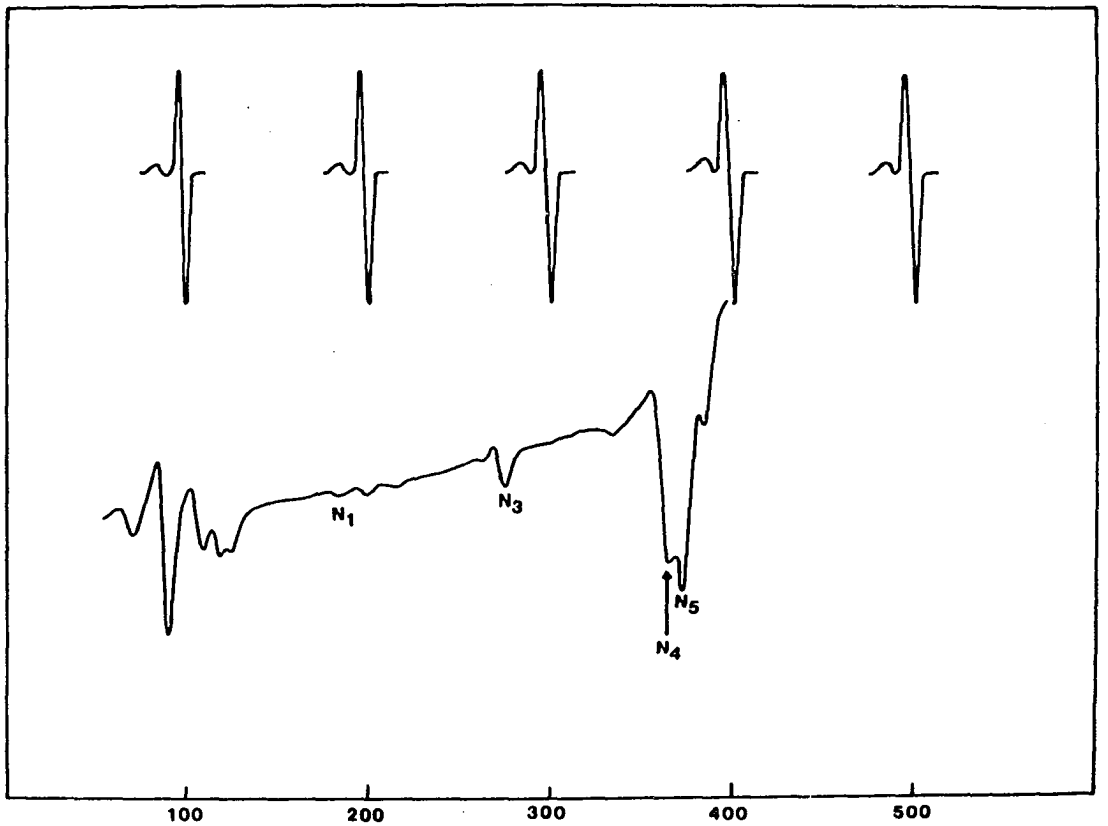

Figure 21. Neodymium major Auger and ionization loss peaks. Primary electron energy was 500 eV.

low energy primary and loss peaks more accurately determine E_I.

For the lanthanide rare earth series investigated, contamination--chiefly from carbon and oxygen--is considerable. Lengthy sputtering produced clean surfaces for Gd-Lu, but the difficulties were greater for the more highly corrosive lighter elements Ce-Eu. Several combinations of sputtering and heating failed to remove all contamination. However, by monitoring loss and Auger peaks for decreasing contamination levels it could be readily assumed that loss peaks at relatively low O coverages were nearly representative of the clean surface atomic energy states.

RESULTS

Atomic energy levels E_W determined from low energy electron ionization loss peaks are listed in Table 3. In general the primary energy was adjusted to produce loss peaks in the 400-500 eV range, since this region is noticeably free of both rare earth and contamination Auger peaks. Parentheses indicate data taken from the X-ray tables of Bearden and Burr[22].

Plasmon loss peaks[37-40] excluded attempts to find the lower energy loss peaks. For the rare earths the O_1-O_3 levels are listed in the X-ray tables as 20-40 eV and were indistinguishable from plasmon losses in the same range.

Table 3

Loss peak and X-ray data for atomic energy levels

	M_4	M_5	N_1	N_2
Ce	899(901)	881(883)	286(289)	(223)
Pr	947(951)	927(931)	301(304)	(236)
Nd	1001(999)	979(977)	315(315)	(243)
Sm	1107(1106)	1080(1080)	345(345)	(266)
Eu	1159(1160)	1131(1130)	362(360)	(284)
Gd	1212(1217)	1184(1185)	375(375)	(288)
Tb	1270(1275)	1236(1241)	392(397)	(310)
Dy	1326(1332)	1291(1294)	407(416)	(332)
Ho	1386(1391)	1347(1351)	433(438)	(343)
Er	1445(1453)	1404(1409)	443(449)	(366)
Tm	1509(1514)	1460(1467)	463(472)	(388)
Yb	1570(1576)	1520(1527)	488(487)	(397)
Lu	1633(1639)	1582(1588)	(506)	(410)

Table 3 (Continued)

	N_3	N_4	N_5
Ce	206(207)	122(110)	122(110)
Pr	215(217)	131(113)	125(113)
Nd	225(224)	136(117)	128(117)
Sm	247(247)	140(129)	130(129)
Eu	258(256)	145(133)	140(133)
Gd	268(270)	149(140)	149(140)
Tb	279(280)	154(147)	146(147)
Dy	290(292)	161(154)	155(154)
Ho	303(306)	166(161)	160(161)
Er	314(320)	175(176)	167(167)
Tm	326(336)	175(180)	175(180)
Yb	345(343)	196(198)	182(184)
Lu	363(359)	213(204)	202(195)

DISCUSSION

It can be seen from Table 3 that there is general agreement between X-ray and ionization loss data for energy levels M_4 - N_3. The higher energy N_4 and N_5 peaks--i.e. for elements Er-Lu--also agree well. For energy levels below about 160 eV, however, there are large discrepancies between loss peak and X-ray values.

It can be demonstrated that ionization loss data is the more useful for surface atoms. Empirical Auger peaks which must be attributed to transitions of the type N_4XX more closely correspond to calculations using ionization loss determinations of E_{N_4} than those based on X-ray energies. This is the case for the $N_4N_6N_6$ transition listed in Table 4, where empirical values and simple $E_{N_4}(Z)$ - $2E_{N_6}(Z)$ calculations employing X-ray and ionization loss data are tabulated. For the elements Ce-Ho the X-ray calculations are in error by an average -10eV. Average error for the same elements using E_W is +1 eV. Furthermore, except Sm and a slight discrepancy for Dy Auger energies by the latter calculation are high, as one would expect, since the unused modification $E'_{N_6}(Z)$ is generally larger than the $E_{N_6}(Z)$ of the above calculations. On the other hand, X-ray calculations are low, and the same modification would only increase an already large error.

The X-ray table lists $N_{4,5}$ as a degenerate level for all the rare earths except the heavy elements Er, Yb, and

Table 4

Auger $N_4N_6N_6$ energies for the rare earths, empirical and calculated using X-ray data and ionization loss data. Calculations are simple $E_{N_4} - 2E_{N_6}$ subtractions.

		Calculated	
	Empirical	X-ray	Ionization loss
Ce	121	110	122
Pr	123	109	127
Nd	130	114	133
Sm	136	118	129
Eu	142	133	145
Gd	142	140	149
Tb	149	142	149
Dy	155	146	153
Ho	160	154	159
Er	157	168	167
Tm	171	169	165
Yb	182	186	184
Lu	183	191	199

Lu (Table 3). The ionization loss peaks indicate non-degenerate N_4 and N_5 for all the rare earths but Ce, Gd, and Tm. Auger doublets of the major peak group are explained by the splitting of N_4 and N_5 levels (Fig. 22). This agrees with the explanation of Coad and Riviere for doublet structure of Auger peaks involving $M_{2,3}$ levels in the transition elements.

Attempts were made to increase the average escape depth of the ionization loss peaks. Unfortunately, for CMA's the necessary increase in energy produces broadening of the peaks and consequent obliteration of fine structure. The result was a single $N_{4,5}$ peak with energy midway between the doublet--e.g. Nd at primary energy 1400 eV produced a single loss peak at 1268 eV; therefore $E_{N_{4,5}} = 132$ eV (Fig. 26). This compares with $E_{N_4} = 136$ eV, $E_{N_5} = 128$ eV for lower incident energy (Fig. 22, Table 3).

The possibility of $N_{4,5}$ level degeneracy in deeper atoms contributing to the ionization loss peak cannot be dismissed. This phenomenon could produce similar results to those reported. Electrons from degenerate $N_{4,5}$, expected to be in the same energy range as the non-degenerate N_4 and N_5 electrons, would add to the overall intensity and could be expected to augment a portion of the $N_{4,5}$ doublet so as to produce a single broad peak. Better energy resolution in the 1-2 keV range ought to determine whether the effect is a materials phenomenon or due to instrumental causes.

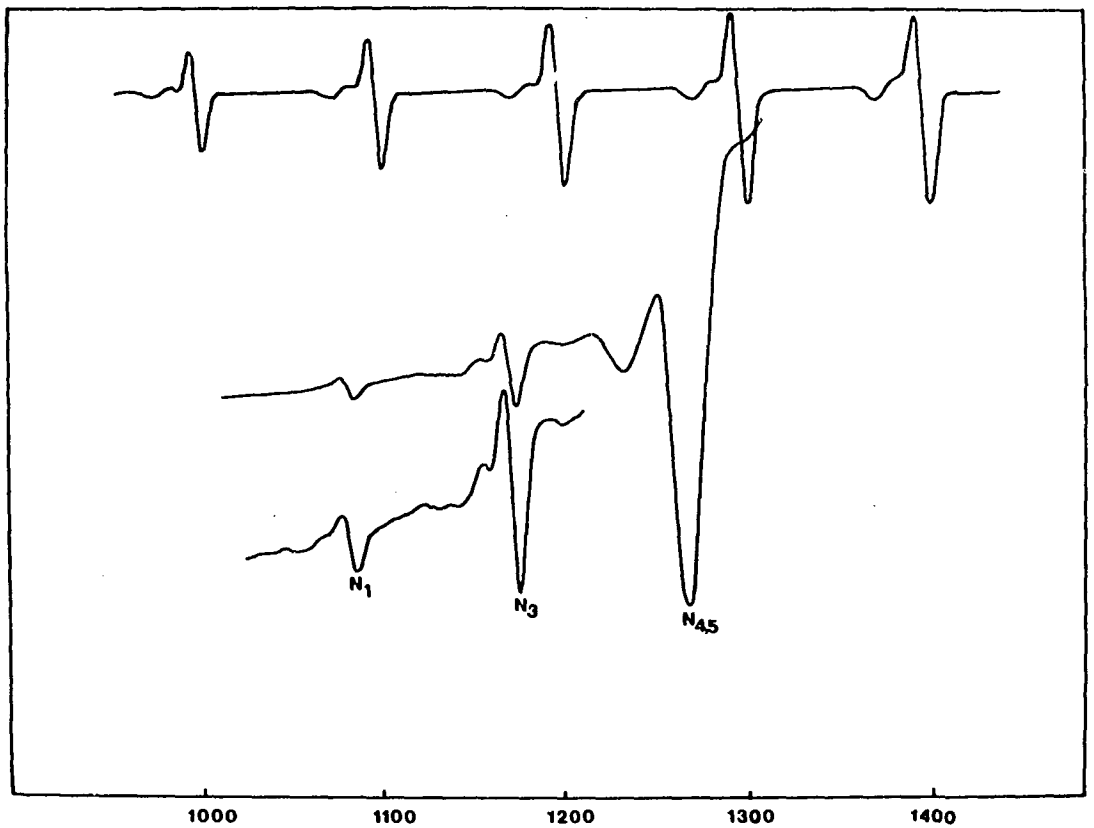

Figure 22. Neodymium ionization loss peaks. Primary electron energy was 1400 eV.

CONCLUSIONS

Lanthanide rare earth N_4 and N_5 atomic energy levels for surface atoms excited by slow electrons disagree markedly with X-ray tabulations. The differences are both quantitative--i.e. N_4 (electron) - N_5 (X-ray) = 11 eV (avg.)--and qualitative (splitting of the N_4 and N_5 levels). The good agreement for the M_4, M_5, N_1, N_3 energy indicates that these discrepancies are not attributable to instrument or discrete loss or gain phenomena.

The findings question Auger peak identifications involving low energy transitions[2,8,29,41,42]. While in many instances it is clear from external evidence or series of data trends that particular Auger transition assignments are appropriate, exact calculations and precise identifications must be justified by direct experimental evidence. X-ray values and extrapolations from such data cannot be considered reliable even given excellent agreement with experiment.

CHAPTER V

AN INTERNALLY REFERENCED CALIBRATION OF AUGER ENERGIES

Auger energies are normally calculated using data from X-ray atomic energy level tables[22,31,43]. Since the Fermi level is referenced as zero energy in these sources, the calculated Auger values automatically assume the same reference. Consistently, empirical Auger energies must also be referenced to the sample Fermi level.

The usual Auger spectroscopic arrangement is shown in Fig. 23. The electron gun is biased, negative with respect to a grounded sample, accelerating thermionically emitted electrons through a potential of generally 0-3 kV. Backscattered electrons (elastically scattered, those due to plasmon and ionization losses, Auger and other inelastic collisions) are energetically discriminated, commonly by LEED modification or the cylindrical mirror analyzer.

An energy diagram of the experimental arrangement is shown in Fig. 24. The sample is grounded. The Fermi level of the electron source filament is biased with respect to the sample Fermi level, zero, by the bias voltage V_B. Electrons are thermionically emitted at total energy ϕ_f.

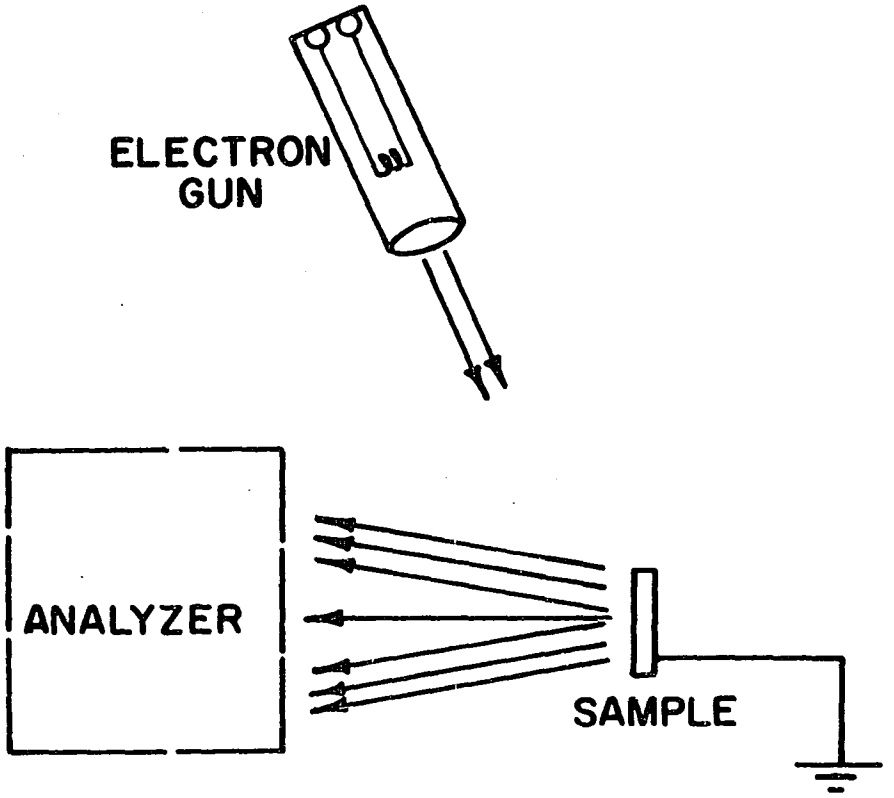

. Figure 23. Auger spectrographic arrangement (schematic).

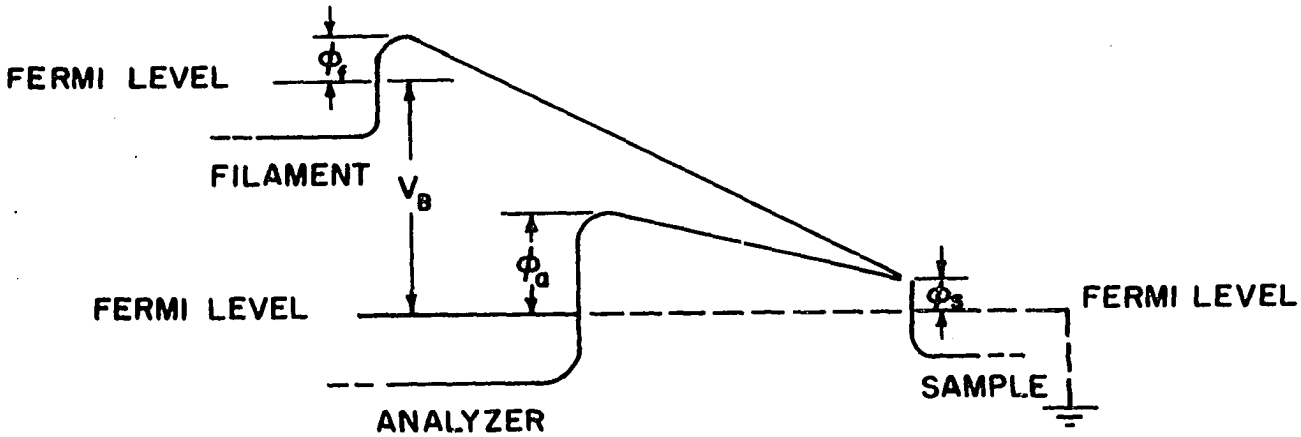

Figure 24. Energy diagram, Auger electron spectroscopy. Shown are Fermi levels, work functions, and bias voltages for filament, sample, and analyzer.

with respect to the filament Fermi energy, or $V_B + \phi_f$ referenced to the sample's Fermi level.

The kinetic energy of an elastically reflected electron just outside the sample surface is the total energy minus the sample work function ϕ_s, or $V_B + \phi_f - \phi_s$. At the analyzer the kinetic energy is modified by the change in the work function barrier between the sample and the analyzer, $\phi_a - \phi_s$, where ϕ_a is the analyzer work function. This analysis excludes instrumental fields applied for the purpose of kinetic energy discrimination. Then kinetic energy of the elastic electron at the analyzer is

$$V_B + \phi_f - \phi_s - (\phi_a - \phi_s) = V_B + \phi_f - \phi_a.$$

Auger electrons may be similarly treated. Let the total, or Auger energy, be E_A. The kinetic energy of the Auger electron in the analyzer is therefore $E_A - \phi_a$. Then Auger energy can be found by adding the work function of the analyzer to the kinetic energy of the Auger peak[13].

The method of calibration presently applied in this laboratory is to use the elastically backscattered peaks as the references for Auger energy (Fig. 25). They provide internal standards which do not require careful measurement of retarding or deflecting voltages or the necessary corrections. Modifications of kinetic energy encountered in the analyzer are canceled, since both elastic and Auger electrons experience the same fields. Furthermore, use of

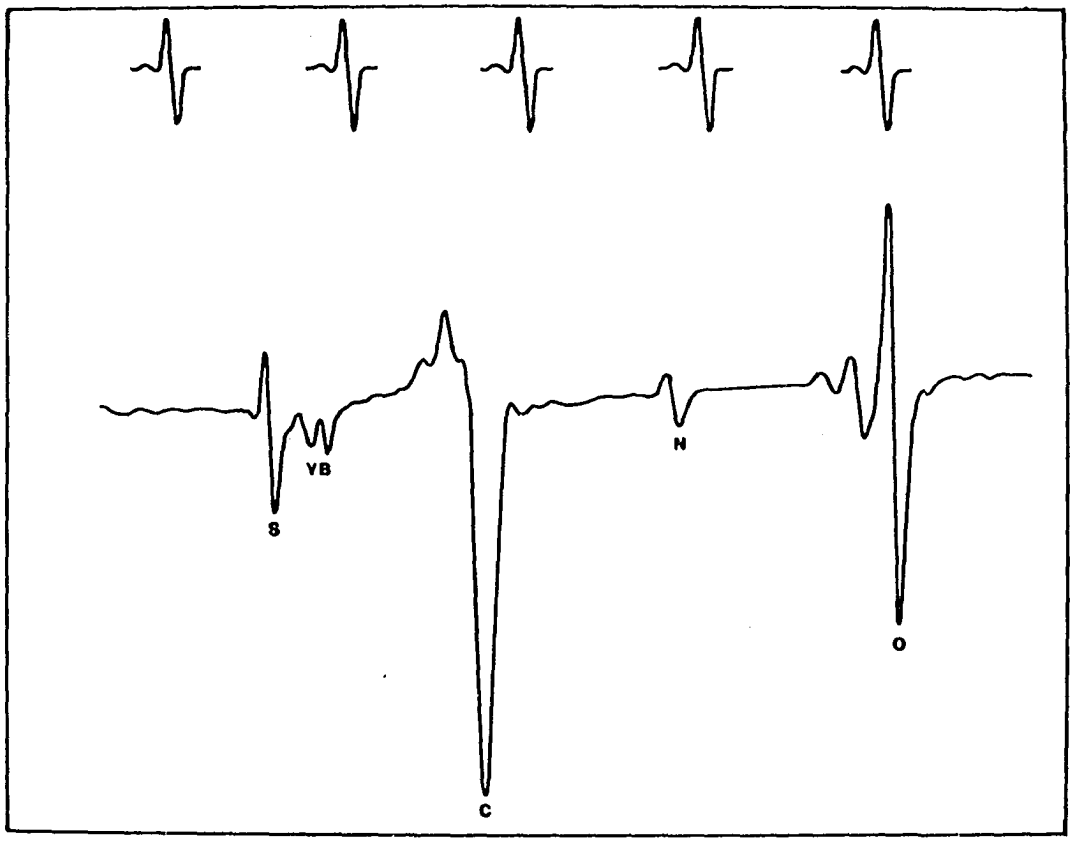

Figure 25. Auger peak calibration. Pictured are contaminant Auger peaks on Ytterbium. Elastic peaks are 104.5, 204.5, 304.5, 404.5, and 504.5 eV.

the differentiated peak minimum for both the differentiated elastic and Auger peaks reduces errors concerning the N(E) Auger peak maximum.

The total energy of the elastic peak is its maximum potential energy $V_B + \Phi_f$. Auger peaks are referenced to the elastic peaks by interpolating between accurately determined bias settings. The necessary correction for the work function is about 4.5 eV for a bare tungsten filament[44]. Using this calibration, some of the more common Auger peaks are listed in Table 5.

The procedure above is similar to the one employed by Askela, Pessa, and Karras[34] using a cylindrical mirror analyzer. Coad and Riviere[36] found that their data obtained with a retarding grid analyzer generally disagreed with that of Askela et al by the constant 4.5 eV tungsten work function. This primary difference in reported energy is not understood. Auger energies found by Yin, Yellin, and Adler[27] using X-ray excitation agree quite well with those of Askela et al. Since X-ray excited Auger transitions were calibrated using well-known photoelectric peaks, the propriety of using elastic peak calibration is indicated.

In summary Auger energies from electron stimulated emission are calibrated for reference to the sample's Fermi level, consistent with theoretical and X-ray work, by the addition of the filament work function. Energies found

Table 5

Auger Energies
elastic peak calibration

S	Ar	C	N	O
152	216 eV	275 eV	385 eV	513 eV

using this calibration are generally 4.5 eV above previously reported data.

REFERENCES

1. I.Bergstrom and R. D. Hill, Arkiv Fysik 8 (1954) 21

2. M. F. Chung and L. H. Jenkins, Surface Science 22 (1970) 479

3. T. W. Haas, J. T. Grant, and G. J. Dooley, Physical Review **B** 1, No. 4 (1970) 1449

4. V. V. Zashkvara, M. I. Korsunskii, and O. S. Kosmachev, Soviet Physics--Technical Physics 11, No. 1 (1966) 96

5. H. Z. Sar-El, Review of Scientific Instruments 38, No. 9 (1967) 1210

6. H. Z. Sar-El, Review of Scientific Instruments 39, No. 4 (1968) 533

7. H. Z. Sar-El, Review of Scientific Instruments 41, No. 4 (1970) 561

8. H. Hafner, J. A. Simpson, and C. E. Kuyatt, Review of Scientific Instruments 39, No. 1 (1968) 33

9. P. W. Palmberg, G. K. Bohn, and J. C. Tracy, Applied Physics Letters 15, No. 8 (1969) 254.

10. L. A. Harris, Journal of Applied Physics 39 (1968) 1419

11. N. J. Taylor, "Basic Auger Concepts", Varian Associates Publication

12. E. N. Sickafus and H. P. Bonzel, "Surface Analysis by Low-Energy Electron Diffraction and Auger Electron Spectroscopy," Ford Scientific Research Staff Publication Preprint, Metallurgy Department (1970)

13. C. C. Chang, "Auger Electron Spectroscopy", Modern Methods of Surface Analysis Symposium, Bell Telephone Laboratories, Incorporated, Murray Hill, New Jersey (1970)

14. P. W. Palmberg and T. N. Rhodin, Journal of Applied Physics 39 (1968) 2425

15. T. E. Gallon, Surface Science 17 (1969) 486

16. M. L. Tarng and G. K. Wehner, "Escape Depth of Auger Electrons", Thirty-Second Annual Conference on Physical Electronics, Albuquerque (1972)

17. G. H. Dieke, Spectra and Energy Levels of Rare Earth Ions in Crystals, Interscience (1968)

18. "Yttrium and the Rare Earths", Michigan Chemical Corporation Technical Bulletin

19. F. Rosebury, Handbook of Electron Tube and Vacuum Techniques, Addison-Wesley (1965)

20. J. V. Florio and W. D. Robertson, Surface Science 18 (1969) 398

21. B. D. Cullity, Elements of X-ray Diffraction, Addison-Wesley (1956)

22. J. A. Bearden and A. F. Burr, Reviews of Modern Physics 39, No. 1 (1967)

23. L. H. Jenkins and M. F. Chung, Surface 26 (1971) 151

24. P. W. Palmberg and H. L. Marcus, Transactions of the ASM 62 (1969) 1016

25. J. M. Charig and D. K. Skinner, Surface Science 19 (1970) 283

26. E. N. Sickafus, Surface Science 19 (1970) 181

27. R. G. Musket and J. Ferrante, Journal of Vacuum Science and Technology 7, No. 1 (1970) 14

28. M. Perdereau, Surface Science 24 (1971) 239

29. W. Haas, J. T. Grant, and G. J. Dooley, Physics Review B 1, No. 4 (1970) 1449

30. J. Strausser, "Varian Chart of Auger Electron Energies", Varian Associates--Vacuum Division

31. K. Siegbahn et al, ESCA; Atomic, Molecular and Solid State Structure by Means of Electron Spectroscopy, Almquist and Wilksalbs Poktryckeri AB, Uppsala (1967)

32. J. T. Grant and T. W. Haas, Surface Science 24 (1971) 332

33. D. Steiner and E. Gyftopoulos, Twenty-Seventh Annual Conference on Physical Electronics, MIT (1967) 160

34. S. Aksela, M. Pessa, and M. Karras, Z. Physik 237 (1970) 38

35. M. Pessa, S. Aksela, and M. Karras, Physics Letters 31A, No. 7 (1970) 382

36. J. Coad and J. Riviere, "LMM Auger Spectra of Some Transition Metals of the First Series", Materials Development Division, Atomic Energy Research Establishment, Harwell, Berkshire, England (1971) AERE-R 0719

37. H. E. Bishop and J. C. Riviere, Journal of Applied Physics 40, No. 4 (1969) 1740

38. P. W. Palmberg, G. E. Riach, R. E. Weber, and N. C. MacDonald, Handbook of Auger Electron Spectroscopy, Physical Electronics Industries, Inc. (1972)

39. L. H. Jenkins and M. F. Chung, Surface Science 24 (1971) 125

40. M. F. Chung and L. H. Jenkins, Surface Science 24 (1971) 649

41. N. J. Taylor, Surface Science 15 (1969) 169

42. H. E. Bishop and J. C. Riviere, Surface Science 17 (1969) 462

43. R. D. Hill, E. L. Church, and J. W. Mihelich, Review of Scientific Instruments 23, No. 10 (1952) 523

44. Chemical Rubber Company Handbook of Chemistry and Physics, Fifty-First Edition (1970)

45. L. I. Yin, E. Yellin, and I. Adler, Journal of Applied Physics 42, No. 9 (1971) 3595

APPENDICES

APPENDIX I

DATA

The rare earth samples used in these studies were one inch square foils from .005" to .020" thick. The more reactive elements were shipped under oil to prevent oxidation. Degreasing followed standard vacuum procedure--successive baths of acetone, trichloroethylene, trichloroethylene, trichloroethylene, methanol, and acetone[19], followed by deionized water rinse and drying. These procedures were conducted under an argon atmosphere for the reactive specimens, and transfer made to the system in an argon-filled plastic bag. The samples were mounted, and the chamber was evacuated. After establishing base pressure of $5 \cdot 10^{-10}$ - $5 \cdot 10^{-9}$ torr, argon sputtering was employed to clean the sample surface.

Electron kinetic energy discrimination using a cylindrical mirror analyzer is sufficiently fast to allow oscilloscope display of an Auger spectrum. This is of great convenience in maximizing Auger intensities. Particularly, sample position produces large effects on signal strength, and therefore specimen manipulation while monitoring oscilloscope display was standard procedure. Phase adjustment for the lock-in amplifier optimizes the differentiation

N(E)/ E and thus the Auger spectrum intensity. Sensitivity settings on the lock-in amplifier, X-Y recorder, and oscilloscope, and voltage to the electron multiplier could be used to vary signal display on either oscilloscope or chart. The time constant on the LIA was normally turned off. Modulation amplitude of the impressed AC voltage was set at 2 V peak to peak. The incident beam current was typically 50 μa.

An initial spectrum was taken from 0-600 eV. This range includes the major peak group, as well as several other rare earth Auger peaks, and those of all the principal contaminants. Auger energies were calibrated, interpolating between elastic peaks set at 100 eV intervals. Fine-grid rectangular coordinate paper aided interpolation and served as a check as to the linearity of the analyzer-recorder signal response. Small or poorly resolved portions of the spectrum were repeated at greater sensitivity. Important parameters, typically beam current, modulation voltage, accelerating voltage, pressure, sensitivity, date, time and cleaning procedures were recorded for each Auger spectrum.

A second portion of the Auger spectrum was taken from 500-1100 eV. In general a sensitivity increase of from two to five times that of the lower range produced large peaks at these higher energies. Other parameters were generally unchanged. Several rare earth Auger transitions produce

electrons of 500-1100 eV; also observed were Fe peaks (on uncleaned samples) and the 513 eV oxygen peak. The 500-600 eV overlap between first and second energy ranges permitted a direct comparison of rare earth Auger intensities using oxygen as a reference standard.

The third spectrum, from 1100-2000 eV, generally required sensitivity settings near the instrumental maximum. Resultant noise increased difficulty in determining Auger energies and tended to obliterate fine structure. Peak broadening as a linear function of energy, inherent in the analyzer, was apparent also. However, this last factor permitted an increase in modulation amplitude--and consequent increase in signal strength--without diminishing resolution further. Several high energy Auger transitions of the heavier rare earths are observed between 1100-1600 eV. No spectra were recorded above 2000 eV, as both noise and slope increase toward the 3 keV (maximum possible incident energy) elastic peak covered Auger signals, if any.

Ionization loss peaks were used to identify Auger peaks and for calculations of the expected transition energies. X-ray atomic energy level tables provided estimates of loss peak energy $E_I = E_p - E_w$, where E_I is loss peak energy, E_p is the primary energy, and E_w is the W level energy recorded in the X-ray tables. Several considerations effect the choice of primary energy. First there is the problem of broadening encountered for the

higher energy peaks. This reduces loss fine structure definition and consequently the accuracy of calculation. Secondly, overlap of loss and Auger peaks must be avoided. Third is the necessity of sensitivity increase and attendant noise as the primary energy--and therefore the beam current--decrease. One would also like to obtain loss peaks as close as possible to their associated Auger peaks so as to nearly equalize electron escape depths. Generally the range 400-500 eV was used for loss peaks. This region is free of contamination and rare earth Auger peaks and represents a compromise among the other energy considerations.

The specimen surface is expected to receive contaminants from the ambient to the extent of one monolayer per hour at an active gas pressure 10^{-9} torr. For this reason the various spectra described above were obtained over several experimental periods. In order to monitor contamination the low energy range 0-600 eV, which includes the C and O peaks, was swept at the beginning and end of experiments. The various spectra could then be compared not only as to contamination levels--rare earth/oxygen Auger intensities, for example--but also as to overall intensity. To improve reliability of the data spectra were repeated at least twice.

Final Auger energies represent averages from spectra meeting contamination criteria. For energies less than 600

eV the observed differences between Auger energy for traces of the same spectrum were less than 2 eV. Above 600 eV the maximum spread was 5 eV.

APPENDIX II

SPUTTER BEAM PROFILE

The rare earth elements required extensive sputtering in order to produce acceptable Auger spectra. To improve cleaning efficiency it was desirable to maximize sputter current density.

There are several rough adjustments which increase sputtering efficiency. Visual positioning was found to produce surprisingly reproducible results. Beam current can be varied by both accelerating and focus voltage controls, as well as filament current. Neither the current density profile or the center of maximum density are determined by simple gun adjustments, however.

In order to profile the sputter beam use was made of a Faraday cup (Fig. 4). The one used in these experiments was constructed from the emitter section of an electron gun. The outer cylinder hole diameter is .020". Ion current passing through the hole was monitored by an electrometer. Total beam current was read from the sputter gun control unit.

A commercially manufactured manipulator (Fig. 5) features linear translation along and transverse its rotation axis. Of the three translations that are paralleling

the axis is the most precise and was used to maneuver the Faraday cup during beam profile experiments. Other degrees of freedom--excluding tilt adjustments, which were not used--provided initial adjustments for the experiments.

The profile was determined by setting sputter gun controls in an Argon ambient of 10^{-4} torr. Common gun control values were total current--10 μa, accelerating voltage--400 V. The sample was rotated and translated across the rotation axis to maximize the current incident on the inner collector. The cup was then lowered by the manipulator to the extreme end of travel along the rotation axis. A precision level was employed to visually determine sample position. Measurements were made through a viewport opposite the sputter gun (Fig. 4), and vertical travel could be read to .05 mm. A table of collected current vs. spectrum position was compiled.

A beam profile plot is shown in Fig. 26. Data points were taken by moving the specimen until a predetermined current change occurred. The one-dimensional plots obtained from sputtering are approximate normal distributions, as expected. The assumption has been made that the true beam profile is simply a rotation about the gun axis of the one-dimensional distribution. This seems reasonable from the cylindrical symmetry of the sputter gun. Furthermore, rotation of the flange-mounted gun by 60° increments produced distributions similar to the original.

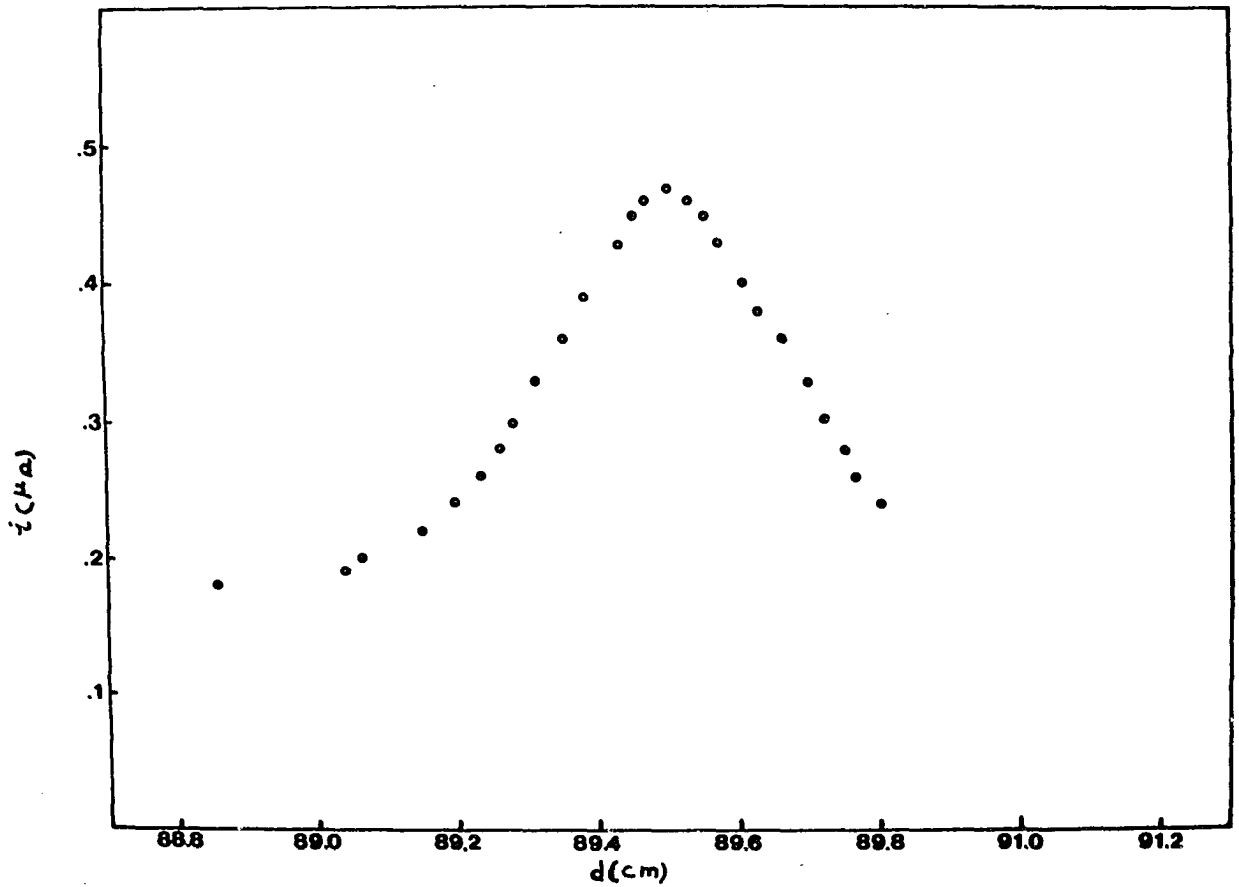

Figure 26. One-dimensional ion sputter beam profile.

A sample's position before the analyzer could be determined to 1mm. A 1mm offset from sputter beam center produces current density about 80% of maximum. For calculating removal rates the 80% maximum current density was used.

Removal rate calculations involve the current density, sputtering efficiency, and atomic density of the bombarded surface. These factors are expressed in the equation

$$r = \frac{ix}{ve\,(\rho A/W)^{2,3}} \quad \text{monolayers/sec.}$$

where i is the incident ion current density, x the sputtering efficiency atoms/ion, v the average valence of the sputter gas ions, e electronic charge, mass density of the sample, A Avogadro's number, and W the specimen atomic weight. For rare earths sputtered by argon, x and v are assumed equal to 1.0, and $\rho A/W$ is about equal to 3×10^{22} atoms/cm^3. The removal rate under standard sputtering conditions is calculated to be 0.1 monolayers/sec.

APPENDIX III

IMPURITIES

The rare earth samples were purchased from Research Chemicals, a Division of Nuclear Corporation of America, Phoenix, Arizona. An optical emission spectrograph had been taken for each lot from which the samples were cut. A summary of impurities is listed in Table 6.

All the samples are rated 99.9% pure exclusive of the processing crucibles, which for these specimens were Ta. Impurity listings do not include oxygen, apparently because the reactive natures of rare earths cause oxygen content to be principally a function of handling. There is doubtless a significant initial oxygen content whatever handling procedures are used upon receipt of the material. Carbon is also assumed to have been present in small amounts in the materials received.

Table 6

	Mg	Al	Si	Ca	Mn	Fe	Y	Pr	Sm	Eu	Gd	Td	Dy	Ho	
Ce	.01*	.01	.01*	.02		.05	.01	.05*							
Pr	.01*	.01*	.02	.01*		.01*		M							
Nd	.01*	.01	.01*	.01		.01*									
Sm	.01*	.01*	.01*	.01*	.05	.01*	.05*		M	.05*	.05*				
Eu	.01*	.01*	.01*	.01*		.01*	.01*		.01*	M	.01*	.01*			
Gd	.01*	.01*	.01*	.01*		.01*	.02		.01*	.005*	M	.01*	.04		
Tb	.01*	.01*	.01*	.01		.01*	.01*				.01*	M			
Dy	.01*	.01*	.01*	.01		.01*	.005*				.1		M	.01*	
Ho	.01*	.01*	.01*	.01		.01*	.08							M	
Er	.005	.01*	.005*	.02		.005*	.001*						.001*		
Tm	.01*	.01*		.01*		.01*							.01*		
Yb	.01	.01	.01	.01*		.03	.005*						.005*		
Lu	.01*	.01*	.01*	.02		.05	.005*								

*No evidence of impurity at this test level.

Table 6 (Continued)

	Er	Tm	Yb	Lu	Ta
Ce					
Pr					
Nd					
Sm			.01*		
Eu					
Gd					.3
Tb					
Dy	.005*				1.0
Ho	.003	.005*	.001*		
Er	M	.02*	.003*		1.0
Tm	.01*	M	.005*		.9
Yb	.008	.005*	M	.005*	
Lu	.005*	.005*	.005*	M	2.0

*No evidence of impurity of this test level.